Quaternary International 638-639 (2022) 180–196

Contents lists available at ScienceDirect

Quaternary International

journal homepage: www.elsevier.com/locate/quaint

Late Pleistocene submarine terraces in the Eastern Mediterranean, central Lebanon, Byblos: Revealing their formation time frame through modeling

N. Georgiou [a,*], M. Geraga [a], M. Francis-Allouche [b], D. Christodoulou [a], P. Stocchi [c], E. Fakiris [a], X. Dimas [a], D. Zoura [a,d], M. Iatrou [a], G. Papatheodorou [a]

[a] Oceanus-lab, Department of Geology, University of Patras, University Campus, 265 04, Rio Patras, Greece
[b] Collège de France, Affiliated researcher, France
[c] NIOZ - Royal Netherlands Institute for Sea Research, Coastal Systems (TX), Utrecht University, P.O. Box 59, 1790 AB Den Burg, Texel, the Netherlands
[d] University of Leeds, School of Earth and Environment, Leeds, United Kingdom

ARTICLE INFO

Keywords:
MIS5
MIS3
Long-term uplift rate
Long-term cliff retreat rate
Sea level change
Marine geophysics

ABSTRACT

Important evidence related to sea-level fluctuation, human evolution and dispersal that took place onshore during the Late Pleistocene and Holocene eras, are currently found underwater due to the sea-level rise. In this study, we present submarine relative paleo sea-level indicators found offshore the Lebanese coastline, at large from the prominent ancient city of Byblos. Two different submarine erosional terrace sequences were identified at depths ranging from −40 to −25m ("distant" sequence) and −11 to 0m ("nearshore" sequence) below present sea level, by using a combination of high-resolution geophysical means and terrain data analysis techniques. In the absence of datings, a model that uses relative sea-level curves for different uplift rates and examines the terraces' formation for various cliff retreat rates (derived from literature and on-field GPS measurements) was built. This model indicates the most possible time frames of the submarine terraces' (STs) formation. The "nearshore" terrace sequence is suggested to have originally been formed during Marine Isotope Stage 5a (MIS5a) sea-level highstand, while it was possibly re-flattened during the first MIS1 sea-level slowdown (8–6 ka BP). The "distant" sequence formation is placed between the MIS4 to MIS3 transition (~62–50 ka BP), and during MIS3 sea-level highstands within 45–35 ka BP. It was also found that a long-term uplift rate of 0.28–0.37 mm/a and cliff retreat rate of 0.03–0.09 m/a best fit our data and existing onshore relative sea-level indicators. The formation of the STs at this time was further supported by chronologically intercurrent uplifting events that facilitated their formation and preservation. Finally, our model supports recent ice-sheet reconstructions related to higher MIS3 values since sea-level curves that were tested for this scenario (eustatically reaching up to −37/−38m depth), proved more successful in the formation of the "distant" sequence.

1. Introduction

Since the Last Interglacial (125ka BP) the global mean sea level oscillated from 6 to 9m above present sea level (apsl) to −125m below present sea level (bpsl) in the Last Glacial Maximum (LGM), due to the relatively rapid growth or decay of the continental ice sheets (Barlow et al., 2018 and references there in). The latter, however, triggered solid Earth deformations and gravitational perturbations in response to changes in the isostatic equilibrium. These, together with other geodynamical processes, caused the local relative sea-level (RSL) changes to deviate from the global mean (i.e., eustatic) (Rovere et al., 2016b). During these sea-level oscillations, the slow rise, drop, or stillstand of the sea level, for at least a short period, are responsible for the formation of Relative Sea-Level indicators (RSLi), mostly during Interglacial periods (Trenhaile, 2002b). RSLi can be formed due to erosion (i.e. marine terraces, notches, etc.), deposition (i.e. beach rock, deltaic sediments, etc.), and bio-construction (i.e. coral reef terraces, algae-vermetid-encrustation, etc.) (Pedoja et al., 2014; Benjamin et al., 2017; Georgiou et al., 2020). The term "relative" reflects the summarized elevation or depth of both sea-level fluctuation and vertical shift of the land since their formation period (Rovere et al., 2016b). However, by the time that sea level rose to the present, great parts of these previously exposed paleo-landscapes were flooded.

The microtidal regime of the Mediterranean Sea along with the

* Corresponding author.
E-mail address: ngeorgiou@upatras.gr (N. Georgiou).

https://doi.org/10.1016/j.quaint.2021.12.008
Received 31 July 2021; Received in revised form 6 December 2021; Accepted 12 December 2021
Available online 13 December 2021

carbonate rocky shores and bioconstruction favors the development of precise and well-preserved paleo sea-level archives (Boulton and Stewart, 2015; Furlani et al., 2014). Thus, the currently submerged areas accommodate a large number of natural paleo-RSLi shaped during previous sea-level stillstands and/or slowdowns, but also archaeological testimonies due to the great maritime tradition (Geraga et al., 2015, 2020; Ferentinos et al., 2020; Georgiou et al., 2021a; Papatheodorou et al., 2021). Although discovering submerged paleo-landscapes is of utmost importance and can be accomplished through integrated methodological approaches (Georgiou et al., 2021b), the literature regarding their existence is quite limited due to the difficulties in mapping, collecting, and dating underwater data (Bilbao-Lasa et al., 2020). This has mainly led to the poor presence of sea-level evidence especially for the Marine Isotope Stages 3 (MIS3), early MIS1, and also of anthropogenic material since the Epipaleolithic-Neolithic periods (Rovere et al., 2011; Furlani et al., 2014; Pedoja et al., 2014; Galili et al., 2017).

The areas that are currently found underwater from 0 to 40m depth in the Eastern Mediterranean were dry for about 60% of the time since MIS7 (~245ka BP) (Galili et al., 2017). Since the cognitive revolution (~70ka BP) the southern Levant coast has been inhabited by Homo sapiens as it was one of the main passages spreading out of Africa, thus it is considered one of the most favorable places for tracking early human life (historic-prehistoric records) (Bailey, 2004; Bailey and Flemming, 2008; Douka et al., 2013; Micallef et al., 2013; Galili et al., 2017).

Lebanon, southern Levant constitutes a tectonically active region which is uplifting all along its coast at different rates (Gomez et al., 2007; Sivan et al., 2010). Vertical tectonic displacement may reduce our ability to estimate the RSL but has favored the preservation of RSLi and especially that of shore platforms, terraces, and notches (Morhange et al., 2006; Trenhaile, 2002a). These RSLi often reflect regional tectonic patterns but they also provide iformation regarding eustatic and isostatic variations (Trenhaile, 2002a; Passaro et al., 2011; Hwan et al., 2013). Apart from tectonic (uplift/subsidence) rates, further information regarding the long-term cliff retreat rates derive when studying the shore platforms (de Lange and Moon, 2005).

In this study, we report the existence of submarine erosional terraces in the offshore coastal area of the city Byblos (Jbeil), Lebanon, Eastern Mediterranean which is known as the most ancient continuously inhabited site and is protected by UNESCO (World Heritage site, 1984). To date, offshore Jbeil is the only area in Lebanon and generally in the Eastern Mediterranean where well-formed submarine terraces are found. The purpose of this paper is: a)to suggest a time frame for the formation of the submarine terraces through modeling which uses as basis marine geophysical data andterrain analysis techniques, and examines their formation possibility for existing relative sea-level (RSL) curves and various cliff retreat and uplift rates, and b) introduce a methodological approach for the detection, analysis, and timing of formation of submerged terraces, lacking chronological framework and dating material, c) to sum up all the available information related to sea-level change in central Lebanon.

2. Regional setting

2.1. Archaeological significance

Ranking among the oldest settlements in a global scale, Byblos was designated a UNESCO World Heritage Site in 1983. Located on the coast of central Lebanon, Byblos had its beginnings in the 5th millennium BC, during the Neolithic period, when fishermen settled on the headland of Byblos, and built simple shelters for protection (Dunand, 194950; Jidejian, 1971). These shelters had evolved into sophisticated circular domestic structures by the Chalcolithic period (7–5.2ka BP) (Jidejian, 1971) and a prosperous fortified Bronze Age city arose on the foundations of the Chalcolithic settlement later on (5.2-4ka BP) an expansion owing to the city's phenomenal economic growth (Grimal, 2009). Ancient Byblos traded and exchanged goods, with every corner of the Mediterranean, as well as with its hinterland and even farther inland with Mesopotamia (Lafont, 2009), mostly accommodating the millennia-long timber trade primarily with ancient Egypt, as shown by many historical accounts and archaeological discoveries, dating to the first Egyptian Dynasties (4.7ka BP). Three offshore anchorages (herein described as "distant" terrace sequence) were located in 1998 (Frost, 1998) and surveyed by (Collina-Girard, 2002), and were thought to have accommodated the large seagoing ships, essential for the city's lucrative maritime trade. A series of Bronze Age stone anchors discovered in the distant anchorage, known as Daaret Martine (Frost, 2002, 2004), does appear to provide support for H. Frost's hypothesis. Recently, the location of the basin of the Byblos Phoenician chief trading harbor was discovered (Francis-Allouche et al., 2017; Georgiou et al., 2018).

2.2. Geological framework & physiography

Lebanon is a tectonically active region and constitutes part of the restraining bend of the left-lateral Levant Fault System (LFS) that separates the Arabian from the Sinai sub-plate. Both plates are moving northwards but the Arabian is moving faster and generates a slip rate of 4–5 mm/a (Gomez et al., 2007a; Reilinger et al., 2006). The Lebanese restraining bend triggered the genesis of the currently growing Mount Lebanon anticlinal structure (Daëron et al., 2004; Nader et al., 2016) and the formation of an extended 30 km offshore thrust system (Mount Lebanon Thrust: MLT) (Fig. 1). MLT is associated with active offshore crustal shortening especially in the area of central Lebanon (Anfeh to Beirut) (Carton et al., 2009), and has contributed to the Mount Lebanon growth since the late Miocene (Elias et al., 2007) (Fig. 1b and c). Central Lebanon mainland is heavily faulted and folded as witnessed by anticlines, by the Qartaba western monocline that runs parallel to the coast, and by the right-lateral WSW-ENE strike-slip faults that divide the area into different structural segments (Asmar et al., 2013; Morhange et al., 2006). The Qartaba structure together with erosion mechanisms (e.g. rivers) exposed the lower lithological unit that consists of Middle Jurassic limestone-dolomite and Upper Jurassic basalts (Fig. 1b and c). This unit is overlain by Cretaceous formations (sand, dolomite, marl, limestone) that cover most of the central Lebanese mainland, while Neogene marl and limestone appear mainly close to the shoreline and east of Mt Lebanon into the Bekaa valley. Byblos ancient city was built on a sandstone promontory overlaying a seaward dipping Cenomanian limestone (Dubertret, 1945, 1954, 1975; Beydoun, 1976).

41% of the Lebanese shoreline is covered by modern structures while about 30% of the remaining coast is rocky (Faour and Rizk, 2008). Its morphology is controlled by the rock properties, marine and subaerial processes (Kennedy et al., 2014; Prémaillon et al., 2018), but also by waves and tide. In Central Lebanon, the mean significant wave height during the spring-summer-autumn seasons ranges from 0.5 to 0.8 m while in the winter months due to the western winds it rises to 1.4m (Kabbara et al., 2006; Aoun et al., 2013). The tide is diurnal (1 cycle every 11h) while the tidal range is about 0.5m (Galili et al., 2017).

2.3. Lebanese rocky shoreline setting

Rocky coasts occur in almost 80% of the world's and half of the Mediterranean's coastline, yet the processes that control them are poorly studied (Furlani et al., 2014; Young and Carilli, 2019). Lithology and tectonics are mainly responsible for the type of the RSLi (marine terraces, notches, etc.) carved on the rocky coasts (Trenhaile, 2015) and for the elevation that they are currently detected (Rovere et al., 2016b), respectively. Lebanon provides good conditions for the formation of RSLi since it has been found that carbonate bedrocks favor their development, and also uplifting landmasses contribute to their preservation especially during interglacial stages (Trenhaile, 2002a; Furlani et al., 2014).

In the model developed for estimating the submarine terraces' (STs) formation time frame, apart from the relative sea-level curves (RSLCs),

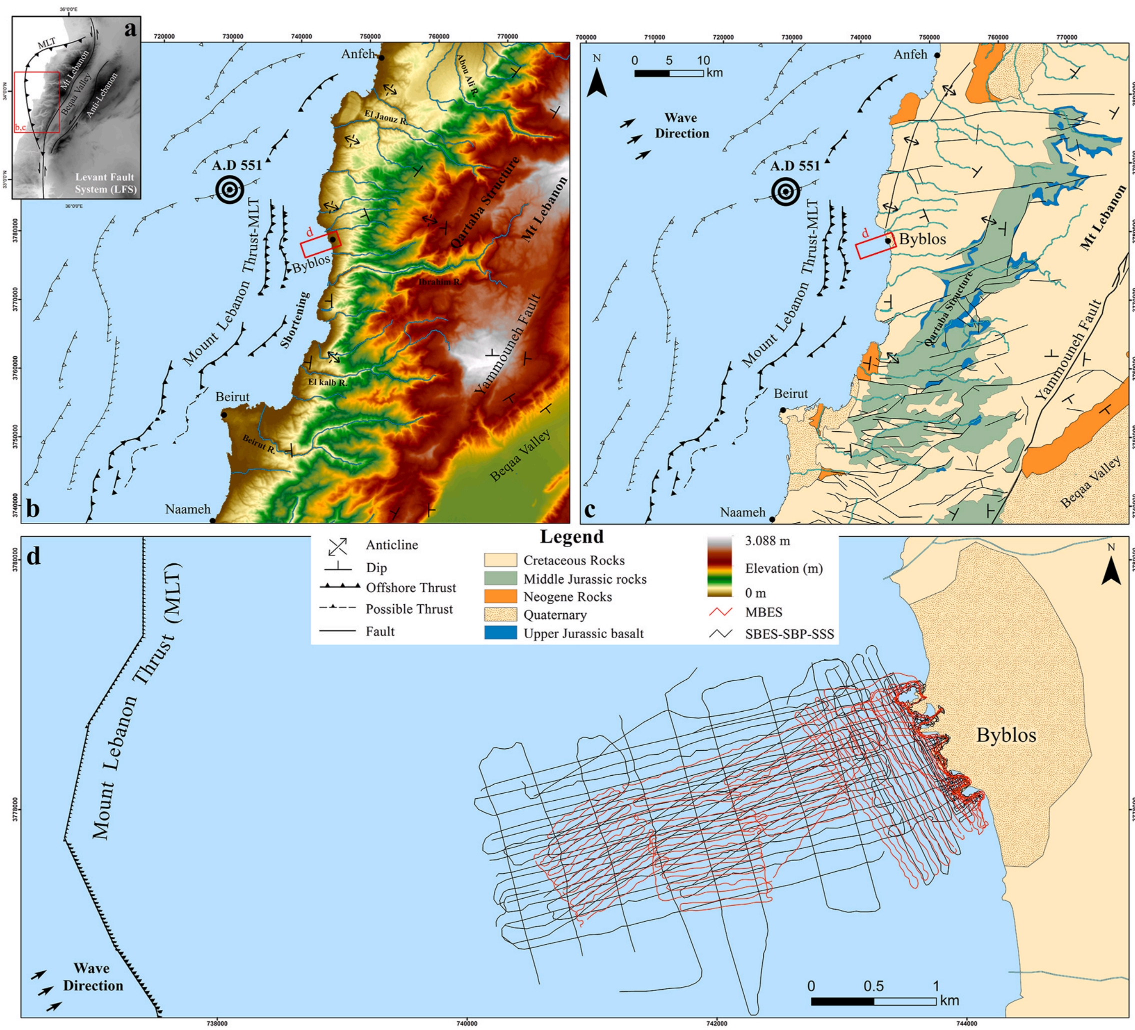

Fig. 1. a) Levant fault system and area of interest (Fig. 1b, c), b) Elevation map showing the Mount Lebanon Thrust-MLT system (Elias et al., 2007; Nader, 2011), the main cities, dips and anticlines, and the A.D 551 seismic epicenter (Plassard and Kogoj, 1981), c) Geologic & structural map showing the fault system, tectonic structures, offshore thrust, main wave direction and area of survey (Dubertret, 1945, 1954, 1975; Beydoun, 1976), d) Marine geophysical track lines performed during the surveys at the offshore area of Byblos city.

the uplift and cliff retreat rate range of the area are used as input. For this reason, it is essential to present existing information regarding the uplift and cliff retreat rates of Lebanon and the eastern Mediterranean in general (sections 2.3.1-2.3.2). To compare our findings with existing RSLi, published RSLi from the MIS1,3,5 are descrcibed in section 2.3.3 (all of the data are presented in detail in Supplementary Tables 1,2,3).

2.3.1. *Coastal uplift*

The offshore thrust (MLT) is believed to be responsible for earthquakes up to 7.5R in the area of central Lebanon, that triggered a tsunami in 551 A.D. (Plassard and Kogoj, 1981) (Fig. 1b and c), while provoking differential uplift of the central Lebanese coast (Gomez et al., 2007; Sivan et al., 2010). The tectonic vertical displacement favored the preservation of RSLi (notches, shore platforms) along the Lebanese coast (Morhange et al., 2006) since raised shorelines along the Lebanese coast revealed two different seismic crises that lasted from 6 to 3 ka BP and 2.7 ka BP to the 6th century A.D. (Morhange et al., 2006). Elias et al. (2007) support that the recent seismic crisis lasted a shorter period, from the 4th to 5th century A.D. Generally, it was assumed that since the 5th to 6th century A.D., vertical tectonic displacement is negligible at the central Lebanese coast (Elias et al., 2007).

Limited surveys revealed that the modern coastal uplift rate is increasing northwards (Israel-Turkey) and was estimated to range between 0.33 and 1.29 mm/a based on fixed intertidal mollusks datings that were developed during the last 3ka (e.g. Dendropoma p.) (Pirazzoli et al., 1991; Sivan et al., 2010).

However, the uplift rate of recently formed RSLi can be overestimated. Gomez et al. (2007) proposed a long-term uplift rate of 0.28mm/a at the area of Tripoli, Lebanon, based on the heights of uplifted non-dated marine terraces, and Elias et al., (2007) proposed a maximum long-term uplift rate of 0.5 ± 0.1 mm/a based on tectonic and geomorphological evidence (Supplementary-Table 1). Generally, in transform zones, the uplift rate is usually below 1mm/a (Pedoja et al., 2014). In the current paper, the same uplift rate range as the modern one is used to explain processes over the last 125 ka, since the study deals with different time scales, accepting that it can be deceiving when used for long-term periods (Stocchi et al., 2018).

2.3.2. *Cliff retreat*

In rocky microtidal areas, horizontal shore platforms (type B) are usually formed within the intertidal zone (Trenhaile, 2006; Sunamura, 2015). On uplifting landmasses, like the Lebanese coast, shore platforms cannot usually reach the equilibrium state, thus the seaward edge of the platform remains relatively static and the cliffs retreat over time (static model) (Trenhaile, 2000, 2001). As a result, the width of the platforms, which is defined as the horizontal distance from the seaward edge to the landward cliff (Stephenson, 2000), provides information about the long-term Cliff Retreat Rate (CRR), which can be estimated by simply dividing the width of the platform with the formation time (de de Lange and Moon, 2005). Modern techniques used for mapping/monitoring cliff recession such as terrestrial-airborne laser scanning and micro-erosion meters proved to be highly accurate. However, these methodologies usually overestimate the CRR (Kennedy, 2016; Matsumoto et al., 2017b; Mushkin et al., 2019). This occurs due to the episodic large cliff failures that accelerate the retreat rate during short-term monitoring periods (Hall et al., 2002).

Although modern techniques provide a precise decadal to centennial CRR, knowledge of long-term field processes and their impacts is limited. Recently, an effort to summarize data on CRR was conducted by Prémaillon et al. (2018) who concluded that median erosion rates range from 0.029 to 0.23 m/a (hard-weak rocks) (Supplementary-Table 2). However, global long-term CRRs in the 20th century A.D. were always $\leq\sim$0.1 m/a (soft & hard rocks) (Mushkin et al., 2019). This rate is included in the long-term mid-Holocene geological and archaeological CRRs (0.03–0.09 m/a) (Barkai et al., 2018) (Supplementary-Table 2). Since i) the last uplifting episode at the Lebanese coast is relatively known (end of 5th to 6th century A.D.) and ii) the platforms follow the static development model (Morhange et al., 2006; Elias et al., 2007), shore platforms' width constitutes a powerful proxy for estimating the long-term CRR (Prémaillon et al., 2018) of the Lebanese cliffs.

2.3.3. Relative sea-level indicators (RSLi)

To date very few surveys that study RSLi along the Lebanese coastline have been conducted. Among the unique findings regarding the MIS1 are the uplifted Dendropoma rims that were found attached on two successive uplifted shore platforms along the central Lebanese coast. These indicators revealed the uplifting regime at least during the last 6ka (Sivan et al., 2010, Pirazzoli, 2005; Morhange et al., 2006). As already mentioned, based on the eastern Mediterranean sea-level indicators, a northward increase in the uplift rate was observed starting from Israel (which is considered tectonically stable) to Turkey (Sivan et al., 2010) (Supplementary-Table 3).

MIS3 sea level constraints are not well studied yet in the eastern Mediterranean. In order for them to be found onshore, the uplift rate should be higher than 1.2 mm/a (Pedoja et al., 2014). Thus, a great part of the MIS3 RSli is currently submerged. Based on proxy-based eustatic SLCs, sea level during MIS3 ranged from −60m to −80m bpsl, with about four 20–30m sea-level fluctuations (Siddall et al., 2008, Dumas et al., 2005; Gracia et al., 2008). In southeastern Israel, hamra deposits of the MIS3 were found at depths starting from 42 to 50m bpsl (Porat et al., 2003; Avnaim-Katav et al., 2012).

MIS5a and 5c RSLi are found underwater in the tectonically stable Gulf of Gabes in Tunisia (8–19m bpsl) (Gzam et al., 2016) and Krk island in Croatia (stalagmites- 14.5m and18.8m bpsl) (Surić et al., 2009) while in Israel, Hamra palaeosols were dated back to 88 ± 18 ka BP at a depth of 22.7m bpsl (Avnaim-Katav et al., 2012). MIS5e RSLi are found from 0 to 49m apsl in the eastern Mediterranean (Galili et al., 2007; Sivan et al., 2010; Dodonov et al., 2008; Tarı et al., 2018). In Naameh, Lebanon, south of Beirut (Fig. 1), a vermetid bench ('trottoir vermet') and Strombus layers were found at an elevation of 8.5–10m apsl and were dated to 90 ± 20ka BP (MIS5a or MIS5c) (Sanlaville, 1969; Leroi-Gourhan, 1980; El Zaatari, 2018). In Lebanon, extended beach deposits appear at an elevation from 45 to 52m apsl (Gomez et al., 2007). Thesedeposits were attributed to Mindel-Riss (MIS11,9?) due to Middle-Acheulean flint artifacts that were found at +52m apsl inside them (Fleisch and Sanlaville, 1974), however, their chronology remains unsure since they haven't been dated yet, so they might also be a result of reworking processes.

3. Material and methods

3.1. Marine geophysical survey & instrumentation

The methodology followed in this article is the result of the combination of different existing methodologies that were originally used for data selection, terrain classification, DEM analysis, and shore platform width analysis. The combined methods followed are described in sections 3.2-3.5, and are supported by a methodological flowchart (Fig. 2).

The original data used for the analysis of the STs were acquired through marine geophysical mapping while the survey track lines followed are shown in Fig. 1d. Three different acoustic systems were used for the marine geophysical survey:

a) An interferometric multi-beam echo-sounder (MBES) (ITER Systems BathySwath1), which covers an area of 150 m of slant range, it has a vertical accuracy of 2 cm while the operational depth reaches 100 m. Simultaneously a single-beam echo-sounder (SBES) was operating at all times to verify the MBES depth. Thus, a Digital Bathymetric Model (DBM) of 70m maximum depth was produced, while that of SBES reached down to 120m depth.
b) A dual-frequency (100 and 500 kHz) Side Scan Sonar (SSS) (EG&G 272TD) was used for mapping the acoustic properties of the seafloor.
c) A sub-bottom profiling system (SBP) (Kongsberg Geopulse) was used for mapping the substrate under the seafloor, providing maximum penetration of 40m, at a resolution of 10 cm. The positioning of the vessel and georeference of geophysical data were provided by RTK GPS (Leica GS08 RTK GNSS) that has an accuracy of 10 mm. Onshore coastal shore platform measurements were also acquired using a Garmin eTrex GPS.
d) During the scuba diving-ground truthing surveys underwater action cameras were used. Samples were also retrieved from the terraces' surface and a macroscopic description was performed.

3.2. Geophysical data interpretation & analysis

The information acquired by the SSS, the SBP, and the ground-truthing survey were used for selecting and delimiting the final DBM. The criteria used for the selection of the area used as the boundary of the spatial extent of the DBM (Fig. 3b- yellow polygon) were i) the areas characterized as rocky or mixed (rocky and slightly sedimentary) (Papatheodorou et al., 2017), ii) with sediment thickness ≤0.5m and iii) that presented high backscatter intensity (BI) in the SSS mosaic. The areas that presented low BI described the presence of loose sediments. This methodological approach but without the use of an SBP for defining the sediment thickness was also used by Bilbao-Lasa et al. (2020) who attempted to identify submerged features in the NE Iberian Peninsula. The methodological approach (section 3.2-3.5) can also be followed in the flowchart of Fig. 2.

3.3. Morphometric analysis

The polygon derived by section 3.2 was used to crop the multibeam DBM and use it as input in the software "TerraceM", developed by Jara-Muñoz et al. (2019). TerraceM aims to map the elevation and spatial distribution of coastal terraces in a semi-automatically controlled environment. More specifically, identification of submerged features was achieved by using a Surface Classification Model (SCM) which enables the user to define topographic slope and roughness thresholds and isolate the flat and smoothed areas. In our case, 5° slope and 0.3 roughness best fit our data, while the DBM resolution was downsampled to 2m cell size. The SCM classified the DBM and produced: (a) an elevation histogram where the distribution of the terraces is apparent, and (b) a spatial distribution map of the classified terraces (Fig. 6). After the terrace recognition, the user is enabled to insert the terraces' paleo-RSL error. In the absence of site-specific data on the modern analog, this error was estimated based on the theory of the indicative

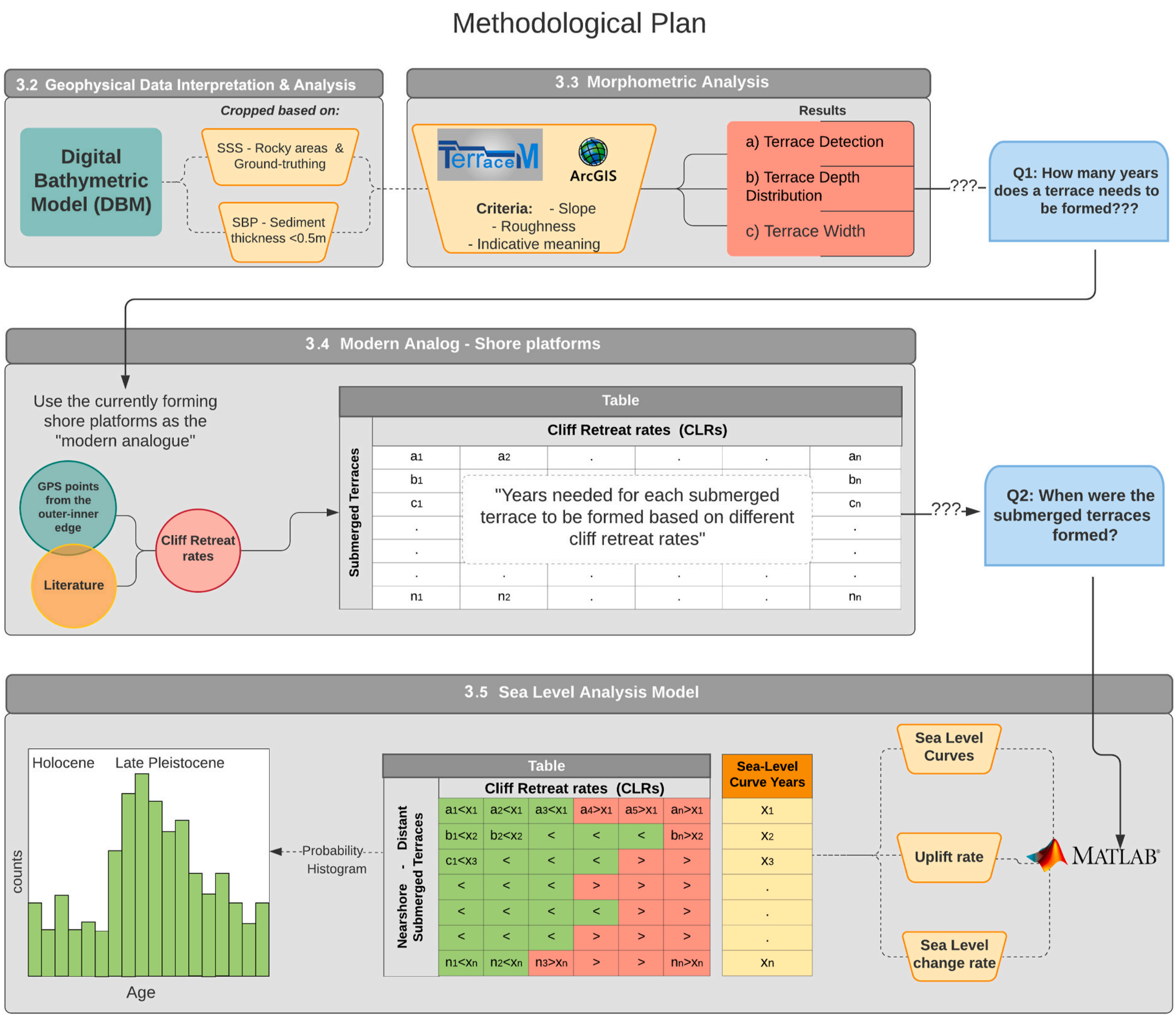

Fig. 2. Flowchart showing the methodologies followed for the analysis of the geophysical data to the construction of the sea-level curve analysis model.

meaning introduced by Rovere et al. (2016a).

To do so, it is necessary to estimate the depth range that the paleo-RSLi were originally formed, assuming that the processes (hydro- and morphodynamic) that are currently shaping the coastal environment are the same as those in the past (Uniformitarianism Principle). Lorscheid and Rovere (2019) created a module ("IMCalc") for researchers to find the information required to calculate the indicative meaning by simply inserting the coordinates and the type of the paleo-RSLi (marine terrace, notch, etc.). In our case, the type of RSLi used was the "marine terrace" that has as an upper limit the "Storm wave swash height (SWSH)" and as a lower limit, the "wave breaking depth (db)". By following the equations proposed in the aforementioned literature the indicative meaning was calculated as follows:

IR = upper limit - lower limit = 0.52 - (−1.02) = 1.54m

RWL =(upper limit + lower limit)/2 = −0.25m

paleo-RSLi = elevation measurement -RWL = elevation measurement +0.25 (Eq. 1)

where *IR* is the *Indicative range* and *RWL* is the *Reference Water Level*.

The results of the terrace detection and depth distribution can be seen in Section 4.2. Finally, the areas identified as terraces in TerraceM software were exported to ArcGIS environment as polygons, towards acquiring information regarding the width and the orientation of each terrace. The width of shore platforms is defined as the extent between the seaward (-outer) edge exposed at low tide and the inner edge at the landward cliff (Stephenson, 2001). In our case, the distant STs do not present the classic staircase morphology that marine terraces present, since they constitute three distinct features. Hence, in order to map the STs the methodological approach for mapping shore platforms of Matsumoto et al., 2017b) was followed. Transect lines that encompassed the outer and inner edge of each terrace were created at a 10m interval while they were oriented based on the inner edge orientation (Fig. 6).

3.4. Modern analog – shore platforms

Before trying to evaluate the formation time frame of the submarine terraces, the question of how many years each terrace needs to be

$$\boldsymbol{paleo-RSLi\ error} = \sqrt{(\boldsymbol{IR}/2)^2 + (\boldsymbol{measurement\ precision}/2)^2} = \sqrt{(1.54/2)^2 + (0.2/2)^2} \pm \boldsymbol{0.6m},$$

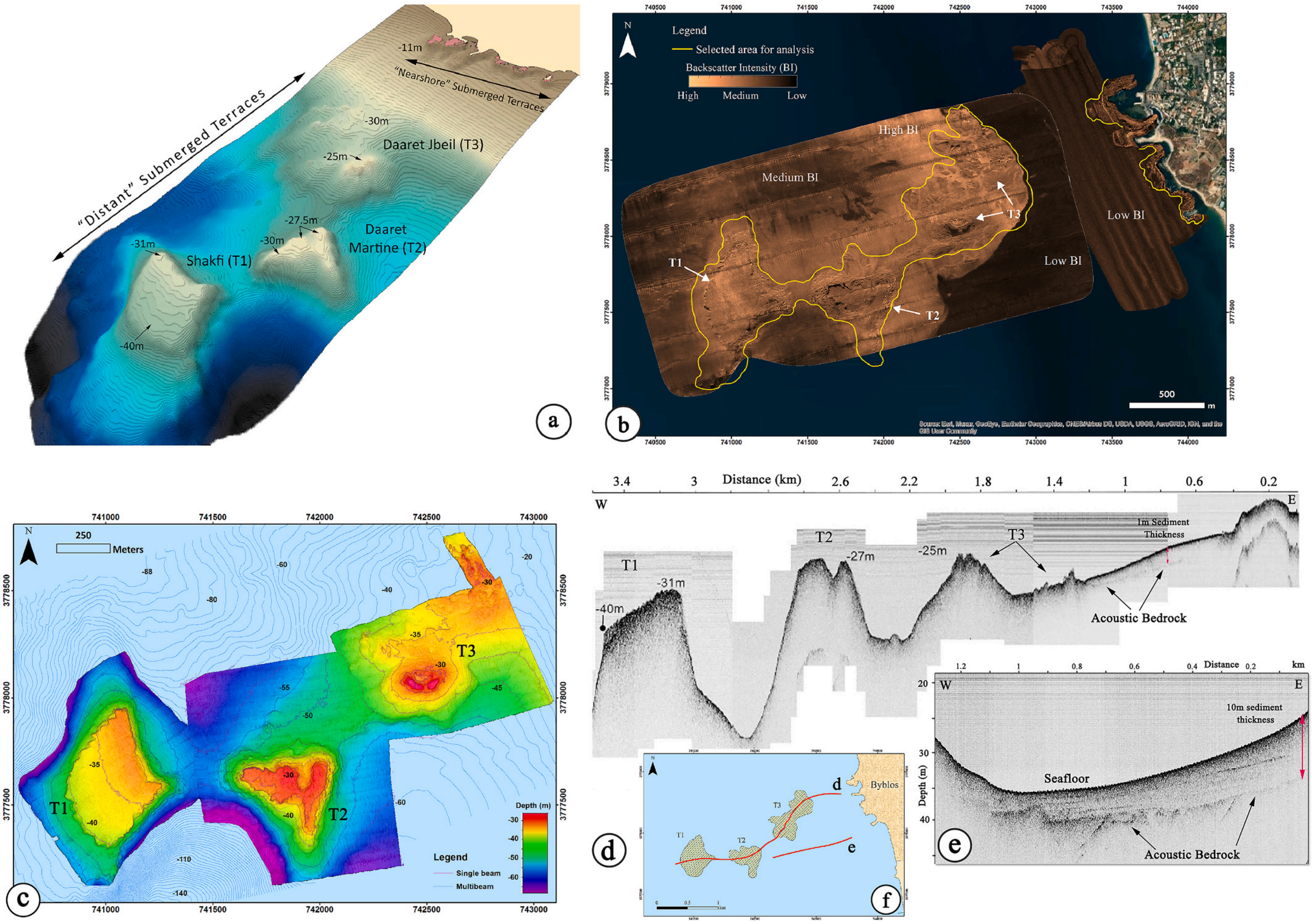

Fig. 3. a) Bathymetry derived by Single-Beam Echosounder (SBES), b) Side Scan Sonar mosaic showing the three distinct submarine terraces (T1,2,3), the backscatter intensity (low, medium, high). The yellow polygon includes the area selected for the model classification analysis and has the following characteristics: <0.5m sediment thickness, high backscatter intensity, rocky formation, c,d) W-E seismic profiles showing the submarine terraces and the limited sediment thickness at a close distance to the terraces and the maximum sediment thickness at the southern part of the survey area, e) seismic profiles location. (For interpretation of the references to color in this figure legend, the reader is referred to the Web version of this article.)

formed should be first answered (Fig. 2- Q1). First, in order to obtain information about the long-term CRR range in our area, CRR of similar formations (sandstone, limestone) around the Mediterranean were retrieved from literature (Section 2.3.2). Since the Lebanese coast is uplifting, the shore platforms haven't reached their equilibrium state (Trenhaile, 2002a). Hence, the width of the currently forming shore platforms can be used as a proxy to calculate the long-term cliff retreat rate (CRR) (or shore platform development rate), and consequently, it could be used as the modern analog for the submarine terraces (STs) (de de Lange and Moon, 2005; Rovere et al., 2016c).

A site-specific survey was conducted at the Lebanese coast. For both Byblos and Anfeh, where different lithologies are met (sandstone, limestone), the width of the shore platforms was calculated. Via using a GPS, the seaward edge and the landward cliff were measured during low and high tide conditions respectively (de de Lange and Moon, 2005; Matsumoto et al., 2017a). Satellite imagery (Google Earth, USGS) was also used to remotely map the shore platforms also during both low and high tide conditions. The GPS measured points were later used as validation points for the satellite mapping (Supplementary-Fig. 2). By delimiting the inner and outer edges it was possible to estimate the mean widths of the shore platforms using also Matsumoto et al. (2017b) methodology, the same followed for the STs width calculation. Since the present sea level (psl) shore platforms have been forming from the last uplifting event onwards (5th to 6th century A.D. onwards, Elias et al., 2007; Morhange et al., 2006; D. Sivan et al., 2010), by simply dividing the shore platform width by the formation time (~1500 yrs) we were able to establish long-term CRR for two different areas and geologic formations in central Lebanon. The CRR both from literature and GPS measurements were compared and taken into account. Without knowing the STs' lithology (sandstone or limestone), different CRRs were used to calculate the time needed for each terrace to be formed. Therefore, simply by multiplying the width of each submerged terrace with each CRR, it was possible to create a table that shows the years needed for each ST to be formed based on different CRR (Supplement- Table 4).

3.5. Sea-level analysis model

Due to the absence of marine organisms' datings from the STs we had to test our geophysical data towards their interpretation as RSLi, for different relative sea-level curves (RSLCs), uplift and cliff retreat scenarios. For this reason, we built a Matlab script that correlates the current depth range of each ST with various RSLCs. Only the parts of the RSLCs where sea-level stabilized or was slowly rising were used while different uplifting scenarios were tested for each RSLC. The eustatic SLCs that were used were those of Waelbroeck et al. (2002); Siddall et al. (2003); Grant et al., 2014 including their upper and lower limits (95% probability intervals) as separate RSLCs (Supplementary-Fig. 1). It should be mentioned that the sea-level curves from Rohling et al. (2014) were also tested but did not contribute to the formation of terraces, thus they were not included in the final results of the model. Moreover, not only did we use the SLC by Galili et al. (2007), describing the RSL the last 10ka in Israel, but we also built two SLCs, predicting the eustatic and isostatic processes of our survey area.

More specifically, all the RSLCs that were used were originally interpolated at a 10-year interval using “pchip” interpolation. After that, an uplift rate that ranges from 0.1 to 1mm/a (at an interval of 0.05mm/a) was attributed to each of the RSLCs (Supplementary-Fig. 1). This uplift rate range derives from literature (Section 2.3.1) and covers both short- and long-term uplift rates. Hence, for each original RSLC, another 19 curves were produced, while in total 200 curves were examined. The uplift rate was attributed linearly, accepting the fact that linear uplift can be deceiving when used for long-term periods (Stocchi et al., 2018).

Terraces are formed mostly during Interglacial periods and for them to be formed sea-level stabilization or slowdown is required for at least a short period (Trenhaile, 2002a). In order to quantify this information in terms of Sea-Level Change Rate (SLCR), we used as a sea-level rise rate limit the only SLCR available which was referred by Antonioli et al., 2015), and Boulton and Stewart (2015) who supported that the notches in the Mediterranean that were originally formed during the Holocene were younger than 6.5 ka BP when SLCR dropped below 5.6mm/a. Hence, by following this criterion, only the parts of the SLCs where the SLCR ranges between 0 and 5.6 mm/a were used.

Finally, the time intervals of each produced RSLC where the sea level coincides with the terraces' depth range were measured in years (example in Fig. 7b) and were then compared to the years needed for the STs formation for the selected cliff retreat rate range (Supplement-Table 4). The periods that verify the years needed for the STs formation were isolated and projected in a frequency distribution plot. By using this sea-level analysis model, it is possible not only to discover the most probable formation period for each ST but also to explore which RSLC, uplift rate, and cliff retreat rate fit best our dataset.

4. Results & discussion

4.1. Byblos coastal geomorphology

Byblos shoreline is characterized by the presence of a sandstone promontory where shore platforms are currently forming at present sea level (Supplementary-Fig. 3). The promontory where the ancient city of Byblos was built, continues underwater for about 4 km to the WSW as it was verified by the marine geophysical data (Fig. 3a,c). West of the shore platforms a submarine “nearshore” terrace sequence extends underwater till a depth of −11m, most likely a sandstone formation as well. The promontory submerges westwards below a thick sedimentary unit of 10m maximum sediment thickness (Fig. 3e). The sediment thickness increases southwards, and is presented on the SSS mosaic as low backscatter intensity (Fig. 3b,d,e,f). The rocky promontory that is buried under the sediments is visible also in the seismic profile and is described as a single continuous enhanced reflector while the sedimentary unit above the substrate is acoustically transparent (Fig. 3d). Further to the West and at the depth of ~30m the previously buried rockybedrock outcrops the sedimentary unit and reaches up to a maximum depth of 25m bpsl (Daaret Jbeil-T3). On this deeper part of the rocky promontory, three distinct rocky flat surfaces were recognized creating an ENE-WSW ridge (T1-2-3). These surfaces were previously known by local fishermen. The eastern one named “Daaret Jbeil” (or T3 in this study) ranges from the depths of 25–30m bpsl. The middle one is called “Daaret Martine” (T2) and ranges from 27.5 to 30m bpsl while the western one is “Shakfi” (T1) and ranges from 31 to 40m bpsl. These flat surfaces are presented on the SSS mosaic as areas of medium to high backscatter intensity while they are surrounded by a thin (maximum thickness 1m) coarse-grained sedimentary unit that appears as high backscatter intensity (Fig. 3b). They probably represent erosional terraces that were formed during different sea-level stabilization and were later flooded by the sea. They do not follow the classic staircase morphology usually known from onshore marine terraces, since they are distinct formations. As observed in the seismic profile the STs are probably carved on the same rock formation with the coastal terraces and the shore platforms since the acoustic bedrock continues from the shoreline to the end of the underwater promontory. However, in the absence of a geologic sample, we assume that the terraces' formation where the terraces are carved is either of sandstone or the underlying limestone. After the depth of 60m, the seabed presents medium to low backscatter intensity while the inclination rises from 2 to 16°, depicting the shelf break.

4.1.1. “Distant” submarine terraces

After the first broad marine geophysical survey (conducted in 2014), an additional terrace-focused survey (2017) was conducted aiming to bathymetrically map the terraces in detail using a MBES. T1 is the deepest and more extended submerged terrace of the study area. It extends 400m from SW to NE and 400m from NW to SE, and it covers an area of $1.6*10^{-1}$ km^2 (Fig. 4a,d). T1 consists of a shallower flat surface on the NE part located at 31m depth and of a sloping surface that inclines to the SW at an average angle of 1.5°. This sloping surface ranges from 32 to 40m at its outer edge. T1 emerges 5 m above the seafloor, it has a lace-type perimeter geometry, and is covered by algal and marine organism encrustation (Fig. 4b and c), similar to the one covering the present shore platforms (Supplement – Fig. 3). Its surface presents a patchy acoustic pattern of medium to high Backscatter Intensity (BI) while partly covered by sand ripples as noted by the 500 kHz SSS mosaic (Fig. 4b). NE and SE of T1 a talus formation is observed consisting of rockfalls until 50m depth. NW and SE of the terrace the seafloor deepens sharply. On the contrary, at the NE and SW, the seafloor slope is gentler and is mostly covered by coarse-grained sandy deposits.

T2 is less extended than T1 (0.054 m^2, 200m SW-NE, 380m NW-SE) and of different geometry (Fig. 4e, f, g). It consists of an upper flat surface at the NE with a depth of 27.5 m (Fig. 4g -B & C), while the rest of the terrace is almost flat and reaches a depth of 31 m at its outer edge. T2 also emerges 5 m above the seafloor and is almost totally surrounded by a rockfall zone except for the SW side (Fig. 4f). The terrace is covered by an algal-marine organism encrustation, while around it the seafloor is covered by sandy coarse-grained sediment as observed by the high BI. T2 is the site where six stone anchors and medieval pottery were found (Collina-Girard and Honor Frost, 2002; Francis-Allouche et al., 2017). The seabed descends abruptly to depths greater than 70 m, especially at the SW, while at the NE the seafloor forms a ridge that connects T2 with T3. The ridge inclines smoothly (<2°) towards the NE and reaches no more than 48 m depth, after which it ascends at a low inclination to connect with T3.

T3 could be divided between the NE and the SW part, due to the different geomorphological characteristics. The SW part is the shallowest (25m) of the “deep” submerged sequence (Fig. 4h). Two algal-marine encrusted rocky outcrops emerge about 5m above the surrounding seafloor, emulating the morphology of sea stacks (Fig. 4h,k). The extent of these two well-preserved rocky outcrops is $4.4*10^{-3}$ km^2 (width 30m-length 80m each), significantly confined in comparison to T1 and T2. A small basin is located at the foot of the two outcrops which is filled by a thin coarse-grained sediment layer based on the high BI and the sediment thickness derived by the seismic profile (Fig. 4i). The surrounding seafloor is covered by soft sediment and outcrops that are also encrusted. East of T3 the low BI delimits the burial of the rocky promontory and the increase of the sedimentary unit. The NE part of the terrace is almost flat and ranges mostly between 31 and 32m, while it reaches 35m in some areas. It displays a patchy seafloor pattern with alterations of rocky outcrops and sand patches (Fig. 4i). It extends 500m from the SW to NE, 400m from NW to SE, and covers $2.65*10^{-1}$ km^2.

4.1.2. “Nearshore” submarine terraces

At the northern coast of Byblos and west of the Medieval harbor, submarine well-developed terraces presenting a staircase sequence were mapped (Fig. 5). Their width ranges from 30 to 100 m, they are also encrusted by algal-marine organisms (Fig. 5c,d,e), while their depth

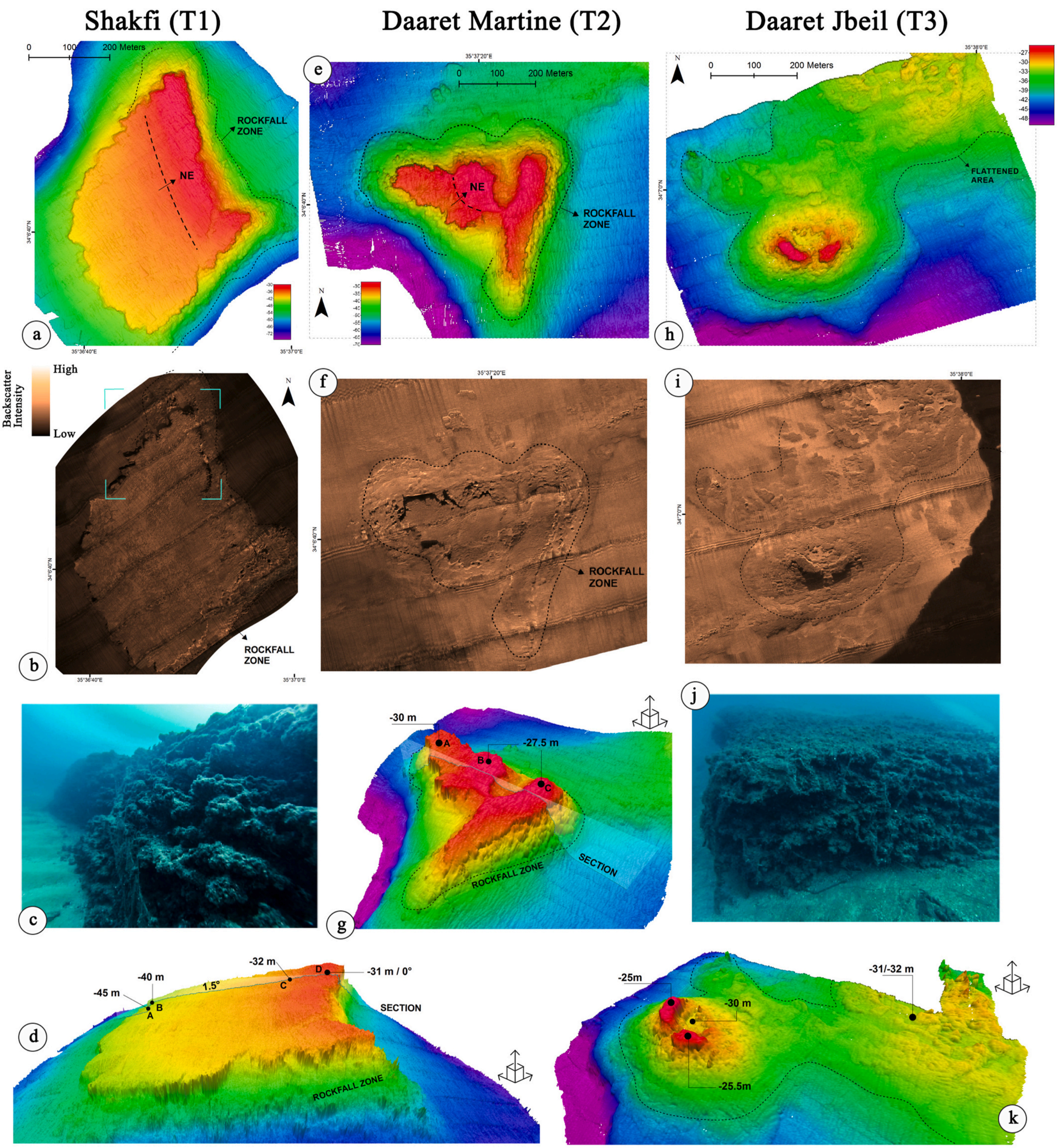

Fig. 4. a, e, h) High-resolution bathymetric maps of the three "distant submarine" terraces (T1,2,3) derived by the Multibeam Echosounder, b, f, i) side-scan sonar mosaics, c, j) underwater photos showing the outer edge of T1 platform (depth 35–40m), d, g, k) 3d bathymetric models showing the depths of the terraces.

ranges from −11.7 to −0.1m (Fig. 5a). South of the Medieval harbor a 140m modern jetty was partly founded (1971) on a pre-existing shore platform. Further southwards, the presence of submarine terraces is reduced while they are succeeded by terraces of smaller width, cliffs, rockfalls, and several notches as observed during the underwater survey. South of this jetty lays the Ras Byblos (or cape Byblos) below the ancient Tell; in this area, submarine terraces are fewer and narrower (20m width; see Fig. 5b). An underwater survey also showed cliffs, rockfall, and wave notches after these successive terraces. In front of bay Jouret Osman and north from Jasmine islet it is the only area where rockfalls are so dense. Submerged abrasion platforms around the islet of Jasmine are very narrow (width 2–5m) and abrasion notches are carved all around the cliff. Some of the notches were likely formed due to sand abrasion at the base of the cliff while others were possibly due to tide or/and wave abrasion (Fig. 5c and d). Although the depth that they are currently detected (1.5m, 3.5m, 5m) matches that of the submerged coastal terraces, their small lateral extent is prohibiting for evaluating them as sea-level indicators. The rest of the seafloor is covered mostly by

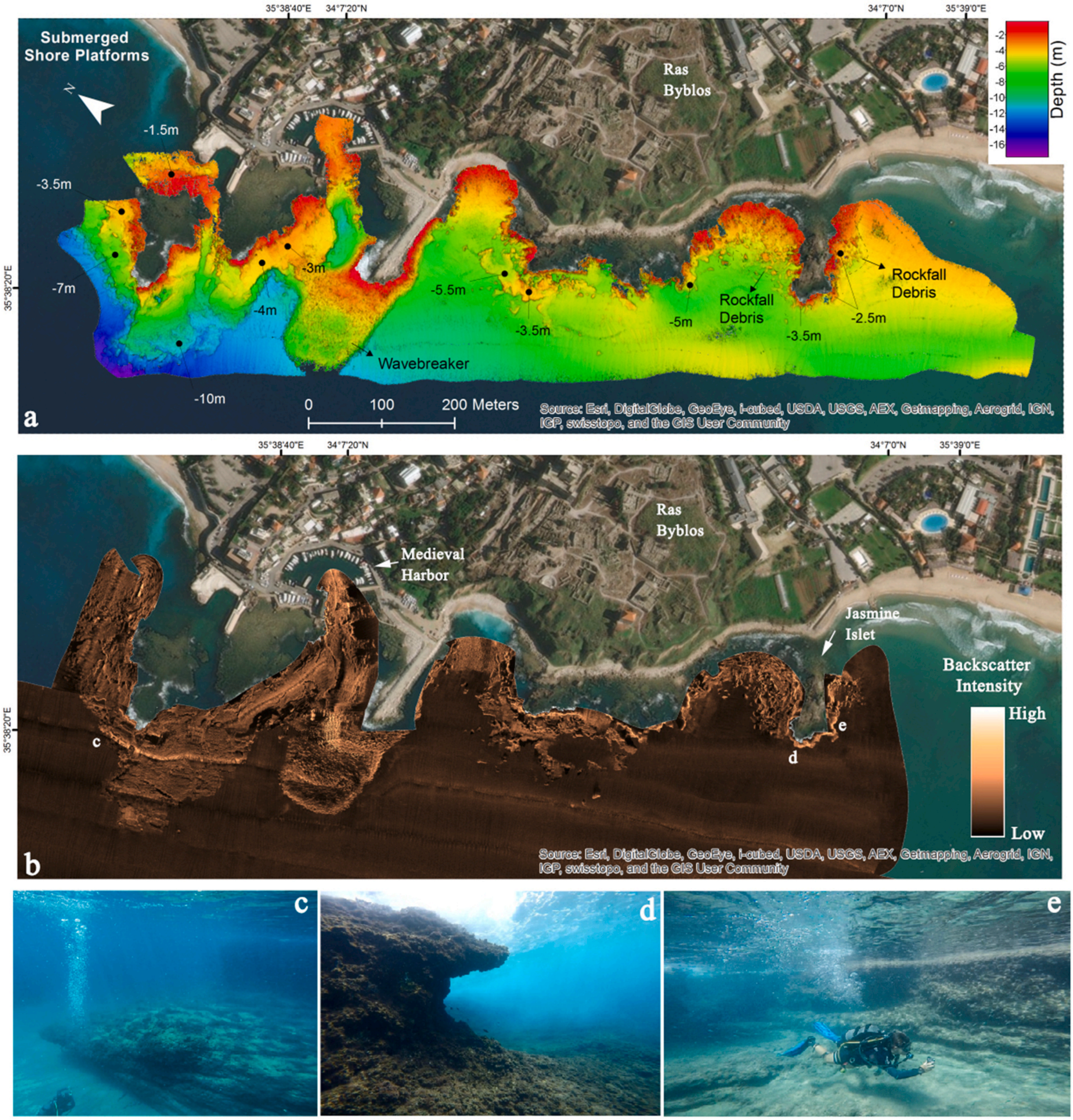

Fig. 5. a) High-resolution bathymetric map of the "nearshore" staircase terrace sequence as derived by the Multibeam Echosounder, b) side-scan sonar mosaic of the same area, c,d,e) underwater photos showing the submerged terraces and underwater notch.

sand. The sandy seabed is intensively affected by the wave and current regime since a 2m depth and 50m width scour, parallel to the shore, is apparent in front of the Jasmine islet.

4.1.3. Shore platforms

As described extensively in the methodological part, the shore platforms of Byblos and Anfeh that are currently forming, on different geologic formations (sandstone, limestone respectively), were mapped through satellite imagery and were validated by measuring the position of the outer and inner edge with GPS in both areas. The shore platforms in Byblos are mainly oriented to WSW (250°) and they are exposed to the main wave direction. They present a mean width of 39 m and they can reach up to 132 m (Supplement -Figs. 2 and 3). The shore platforms north of the breakwater are better-developed and of greater width than those south of it, as seen above. Also, as stated earlier, the outer-seaward edge is well-developed and is delimited by an elevated algal rim which acts like a wave-breaker. The exposed part of the shore platforms is coated by algal organisms.

On the contrary, shore platforms that are formed on limestone in the area of Anfeh, are pretty confined (Fig. 2). The mean width is 20m while

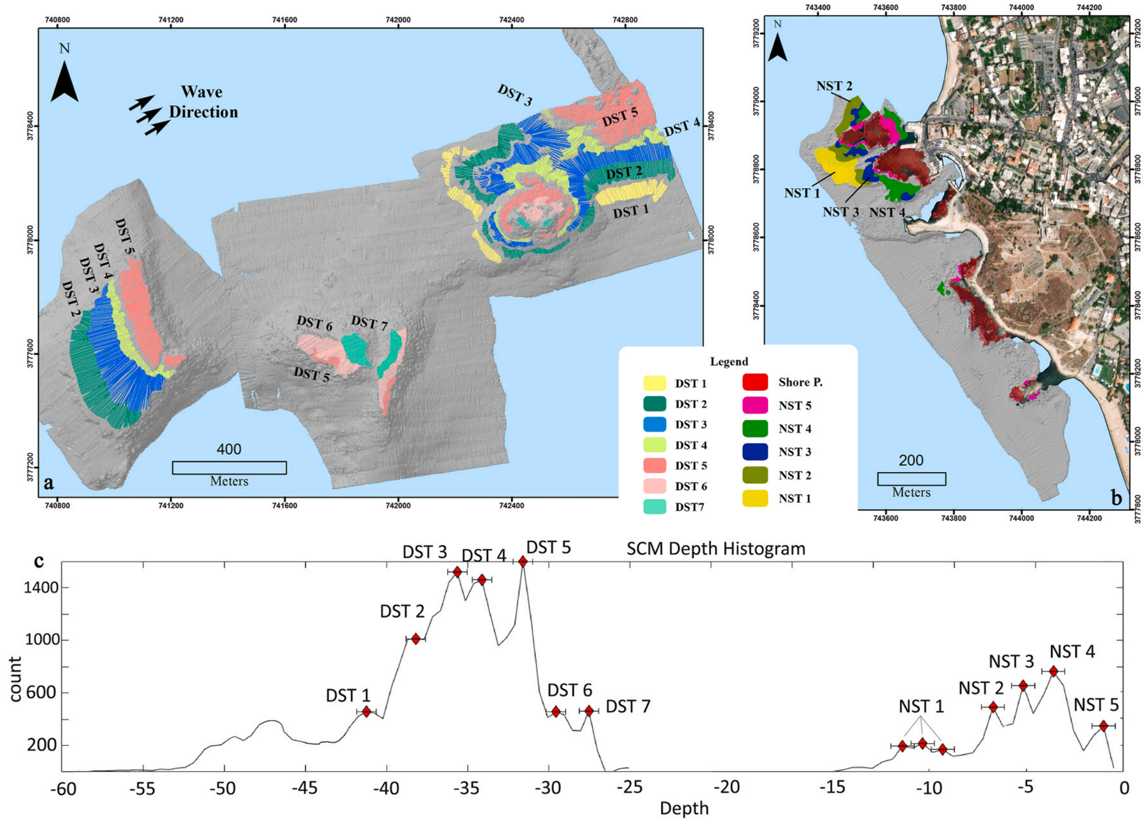

Fig. 6. a,b) Terraces detected and classified by TerraceM software (Jara-Muñoz et al., 2019), c)Terrace depth distribution histogram.

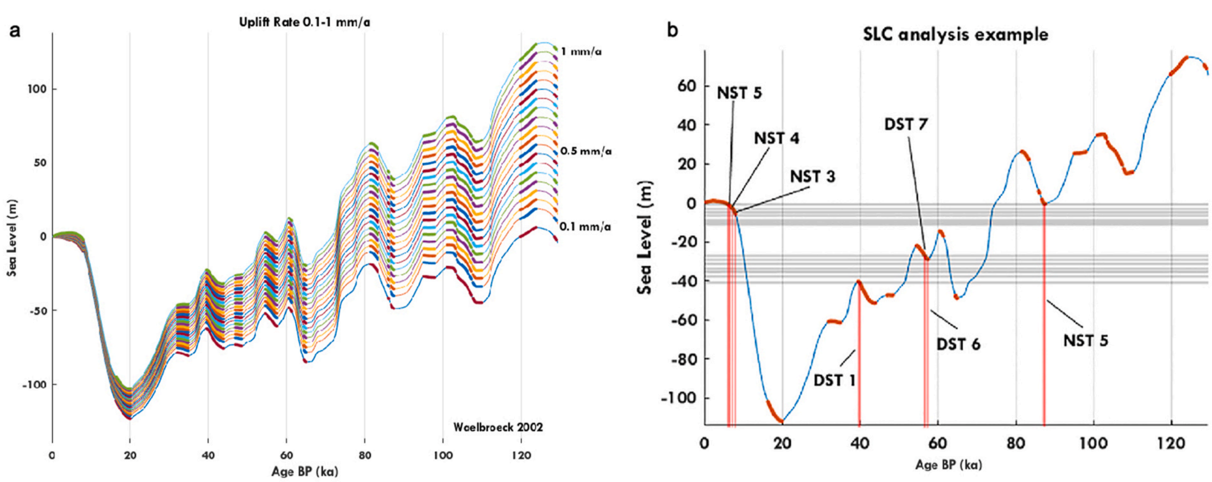

Fig. 7. Example of Waelbroeck et al. (2002) sea-level curve used as input in the sea level model with different uplift rates. Thick lines are the part of the sea-level curves that fulfill the criteria set by the model, b) plot showing the part of one sea-level curve that fulfills the criteria set by the model, in comparison to the depth of each submarine terrace.

the maximum width reached up to 60 m. The platforms are distributed at both sides of the rocky promontory, thus their orientation ranges from 250° to 350°. The seaward edge is also apparent, however, the shore platforms in Anfeh almost lack the presence of an enhanced algal coating and an elevated biological rim. Also, the presence of potholes along the Anfeh coast is more significant than that of Byblos.

4.2. Terrace detection and analysis

As widely explained in the methodology, for the detection and analysis of the submarine terraces a Surface Classification Model built in the TerraceM software was used (Jara-Muñoz et al., 2019). The rocky areas and those buried under a maximum of 0.5 m sediment thickness (Fig. 3b-yellow polygon) were extracted from the original bathymetry DBM and were used as input for the classification model. For the identification of the submarine terraces, threshold values of 5° slope and 0.3 roughness best fit our data. A depth distribution histogram was then built based on these thresholds (Fig. 6c). The histogram showed a roughly symmetric, left-skewed, almost unimodal elevation distribution. The frequency distribution showed an unambiguous increase in the presence of terraces between 40 m and 30 m depth. Five different peaks, thus five different terraces were noted at −41, −38, −35.4, −34, −31.3,

−29.3, −27.3 m bpsl (DST1-7, Fig. 6a) with an error of ±0.6m. The same methodology was followed for the detection and analysis of the nearshore submarine terraces. Using the same thresholds, the depth distribution histogram showed also a roughly symmetric, left-skewed, almost unimodal elevation frequency distribution. The greatest presence of terraces was observed at a depth ranging between 7 and 0.5 m as five different terraces were noted at −11.1, −6.4, −4.9, −3.3, −0.7 m depth NST1-5, Fig. 6b) with an error of ±0.6 m.

After the terrace detection and analysis, the mean width of each terrace was estimated in the ArcGIS environment based on 10m interval transects. The depth range (corrected for paleo-RSL value and paleo-RSL error, see section 3.3) and mean width of each terrace and shore platform are presented in Supplement Table 4.

4.3. *Chronological framework – sea level curves analysis & formation time frame*

The problem of the submarine terraces' formation period could not be resolved due to the lack of dating material from these STs. For this reason, a script that analyzes already published RSLCs and examines the sensitivity of our database for different uplift and cliff retreat rates was built (Section 3.5). To make the script flow reader-friendly an example of one RSLC is presented below (Fig. 7). 19 different uplift rates were attributed linearly to the RSLC of Waelbroeck et al. (2002) resulting in a total of 20 RSLCs together with the original (0 mm/a uplift) (Fig. 7a-thin lines). The script isolates the parts of each RSLC where sea level rises at a rate of 0–5.6 mm/a (Fig. 7a-thick lines). Secondly, the parts of the RSLC

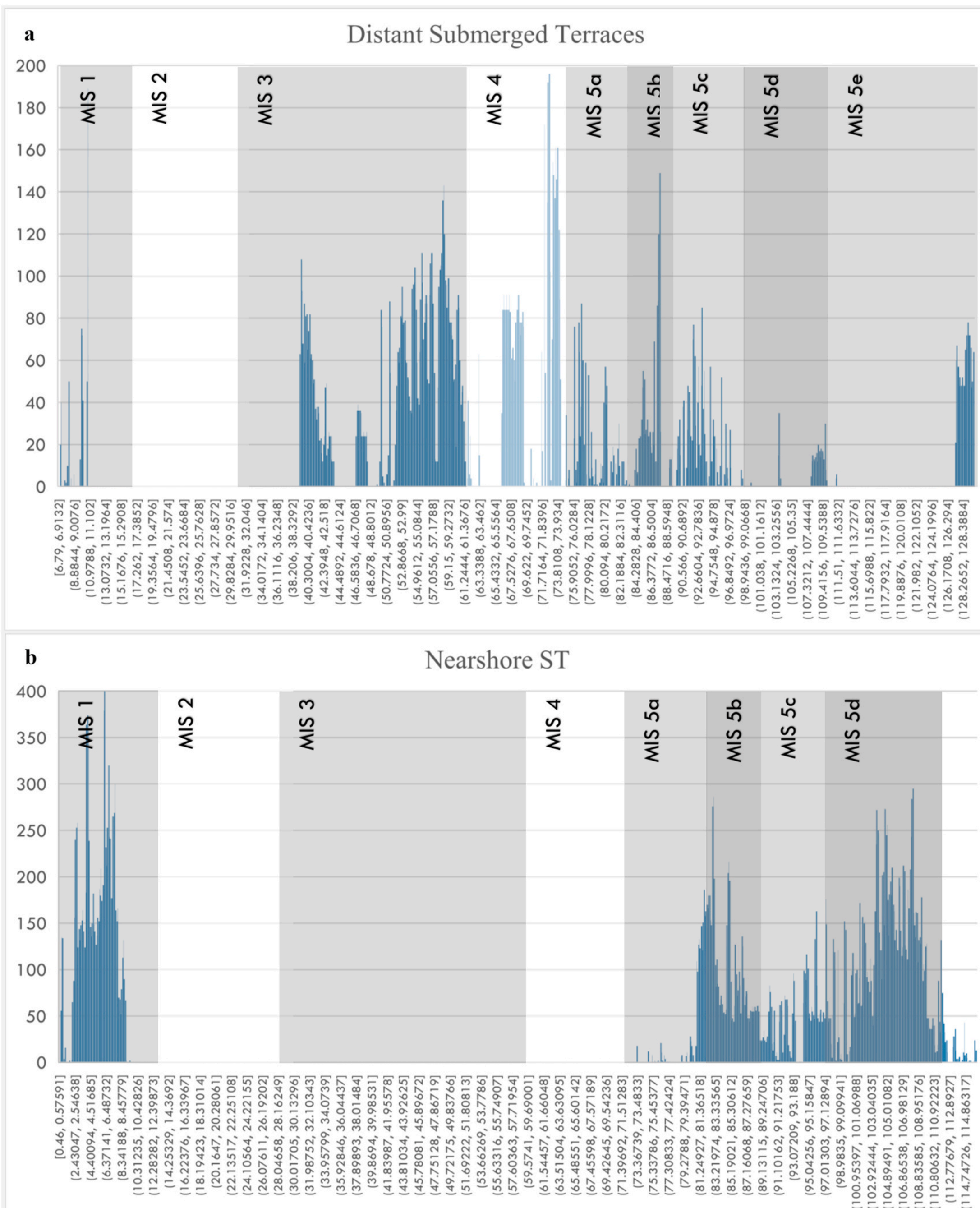

Fig. 8. a) Frequency distribution plot showing the time periods when the formation of the"distant" submerged terraces is more probable, b) Frequency distribution plot showing the periods when the formation of the "nearshore" submerged terraces is more probable.

that were isolated and coincided with the depth range of each ST were counted in years (Fig. 7b-thick red lines) and were compared to the years that each ST needed to be formed for different CRRs (Supplement--Table 4). The values that confirmed the predicted values from the modeled RSLC were considered "successful" (Fig. 2, section 3.5). Hence, the periods when the formation of terraces is successful were extracted and projected in frequency distribution plots (Fig. 8). The script was set to run in a loop in order to test all the available RSLCs separately.

In Fig. 8 are projected the successful periods' frequency distribution from all the available RSLCs used in the script, thus the periods when stabilized or slowly rising sea-level coincides with the distant STs' depth range and as a consequence when the formation of the STs' is more probable. The two plots refer to the distant and nearshore STs tested for the long-term uplift rate range (0.28–0.5 mm/a) (Fig. 8a and b). Although the results regarding the distant STs are more scarcely distributed, the average value remains close to the one derived from all uplift rates and is 64.34 ka while the median is 61.36 ka (Fig. 8a). The highest probability is apparent mainly during MIS3 and between MIS4 and MIS5a. The histogram of the nearshore STs is also multimodal (Fig. 8b) but it is well determined. The data are concentrated in two different periods, MIS1 and MIS 5. The data in MIS1 range between 0 and 9ka while those of MIS5 present two different maxima, one at about 83ka (MIS5a) and the other at 106ka (MIS5c).

The "success" of each uplift rate, thus the amount of the predicted ("successful") RSLC years were also projected, resulting in the creation of a bar chart showing the uplift rate in X-axis and the success of each uplift rate in normalized values in Y-axis (Fig. 9). The success of each uplift rate for the distant STs is shown in blue color and for the nearshore STs in green color. The success of the nearshore STs is moderate (<0.6) for uplift values of 0.1–0.25 mm/a while the highest values (0.7–0.8) appear from 0.3 to 0.45 mm/a. This uplift rate range coincides with the long-term uplift rate derived from the literature. As the uplift rate grows from 0.5 to 1 the success of our model drops. Regarding the distant STs, the model's success is generally low (less than 0.3). It was observed that for the uplift rates that the nearshore STs were highly successful, the corresponding distant STs were not (<0.2).

5. Evaluation of findings

5.1. Comparing long-term cliff retreat & uplift rate, and RSL indicators

It is widely known that the CRR and the width of the shore platforms are mainly dependent on the rock lithology and material strength (Sunamura, 2015). Considering that the last uplifting episode at the Lebanese coast is relatively known (end of 5th to 6th century A.D.) and that the shore platforms follow the static development model (Morhange et al., 2006; Elias et al., 2007), their width constitutes a powerful proxy for estimating the long-term CRR (Prémaillon et al., 2018). An effort was made to assess the current CRR along the Lebanese coastal zone by measuring the width of the shore platforms via GPS in two different areas, of different lithologies, at Anfeh and Byblos. We estimated that the CRR of Anfeh's limestone was estimated at 0.013 m/a and that of Byblos sandstone at 0.026 m/a. These rates are generally considered low. However, they are similar to the ones calculated from Israel (eolianites-paleosols) and by mid-Holocene geological and archaeological indexes (0.03–0.09 m/a) (Barkai et al., 2018; Mushkin et al., 2019). Furthermore, our model confirmed the formation of the nearshore STs by using the existing RSLCs for CRRs of 0.03 and greater (Supplement-Table 5)

The long-term uplift rates usually derive from direct measurements of MIS1 and MIS5e RSLi (archaeological and geological), especially in tectonically stable areas. As a result, sea-level fluctuations during these periods are better constrained (Sivan et al., 2001). The formation of the nearshore STs in our survey area coincides with the MIS5 and/or MIS1. Our model showed that the nearshore STs were more likely to be formed when using uplift rates that ranged between 0.3 and 0.45 mm/a (Fig. 9). This rate coincides with those of Gomez et al., 2007) (0.28 mm/a) and Elias et al., (2007) (0.5 ± 0.1 mm/a), calculated based on geological and tectonic evidence.

Apart from the work of Sivan et al., (2001), RSLi formed since previous Interglacial periods are very scarce. The only MIS5 RSLi found close to our survey area (Naameh, south of Beirut) was a vermetid bench and Strombus layers at an elevation of 8.5–10m apsl, dated to 90 ± 10 ka BP and 90 ± 20 ka BP respectively (Leroi-Gourhan, 1980; El Zaatari, 2018). This date indicates two possible periods of formation, either MIS5a or MIS5c interglacial periods. By taking into account that sea level during MIS5a was about −19m bpsl (~85ka BP- Barbados) (Schellmann et al., 2004) and MIS5c (~100 ka) was about −21m bpsl (Potter et al., 2004), long-term uplift rates of 0.32–0.34 mm/a and 0.29–0.31 mm/a respectively, would be needed for these RSL indicators to be uplifted into the present elevation.

5.2. Submarine terrace formation time frame

5.2.1. "Nearshore" submarine terraces

The nearshore STs are found at depths from 0.1 to 11.7m bpsl. As

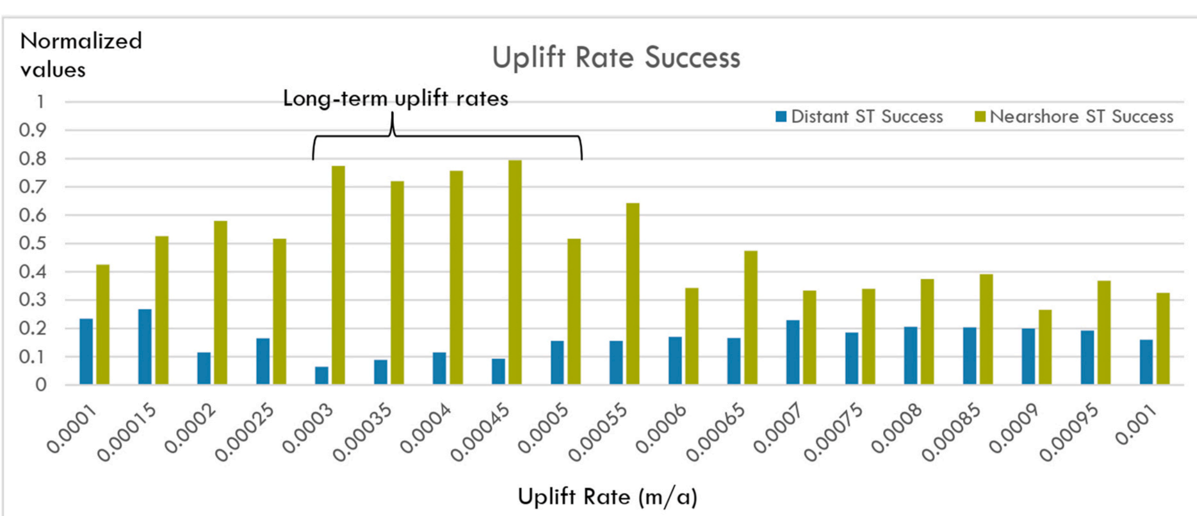

Fig. 9. Success rate (normalized) of each different uplift rate used in the model (distant STs: blue color, nearshore STs: green color). (For interpretation of the references to color in this figure legend, the reader is referred to the Web version of this article.)

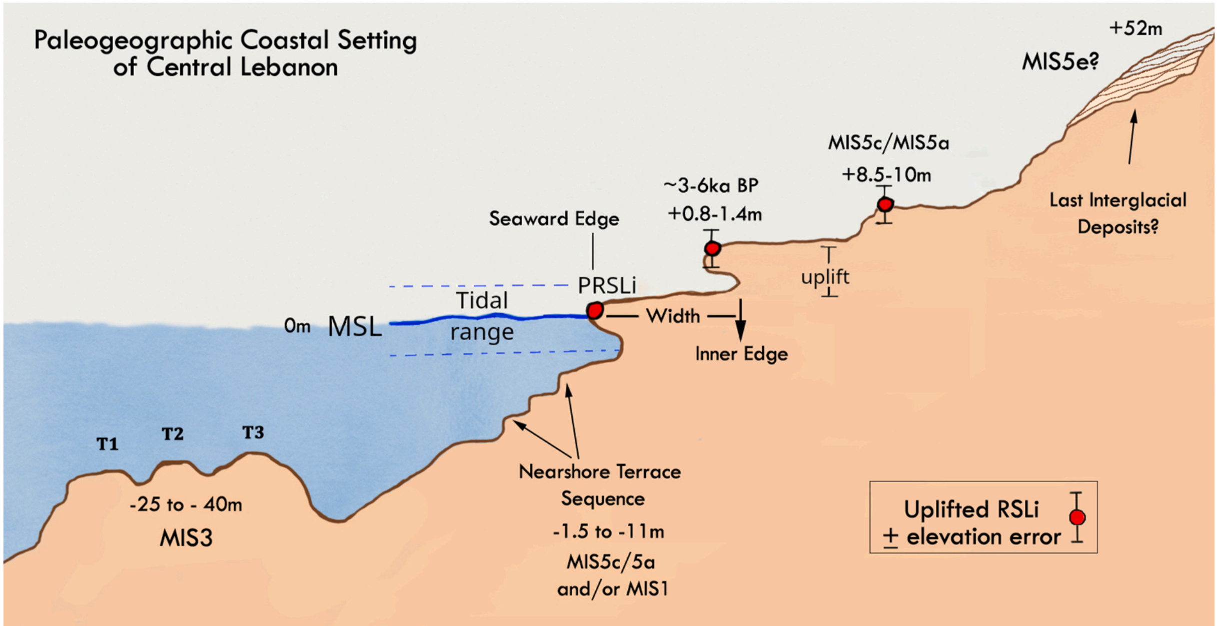

Fig. 10. Descriptive sketch of the paleogeographic coastal setting: currently forming shore platform, uplifted shore platform, submarine terraces and sediment deposits of the coastal zone as described in sections 2.3.1-3. (PRSLi: present relative sea-level indicators, RSLi: relative sea-level indicators. Uplift rate is determined as: uplift rate= (RSLi elevation-PRSLi elevation)/(RSLi age- PRSLi age) and cliff retreat rate as: CRR = width/RSLi installation age). Elevation error and sketch are not in scale.

derived by the RSLC analysis (Fig. 8b), the periods that favored their formation were the interglacial MIS1, MIS5a, and/or MIS5c (Fig. 10).

By taking into account the following facts:

a) the formation age of the rock where the STs were carved is not known (before or after MIS5),
b) an uplifted vermetid bench of MIS5a or MIS5c possible formation age is found onshore at an elevation of 8.5–10m (Sanlaville, 1969; Leroi-Gourhan, 1980; El Zaatari, 2018), and that
c) uplifted terraces that were formed from 6ka onwards are found uplifted onshore (Sivan et al., 2010, Pirazzoli, 2005; Morhange et al., 2006), we are allowed to make two alternative hypotheses:

i) In the first hypothesis, we assume that the vermetid bench found onshore (Sanlaville, 1969; Leroi-Gourhan, 1980; El Zaatari, 2018) was constructed during the MIS5c and that the rock formation age is older than MIS 5c. Hence, the nearshore STs could have originally shaped during the highstand MIS5a and/or re-flattened at sea-level stabilizations and/or slowdown during the upper phases of MIS 1 (~8-6ka BP) (Fig. 10).
ii) The requirement for the second hypothesis is that the uplifted vermetid bench referred in previous "fact b" (Sanlaville, 1969; Leroi-Gourhan, 1980; El Zaatari, 2018) was built during MIS5a. Thus, all the nearshore STs were formed during the more recent interglacial period MIS1. However, this scenario cannot be currently supported by our data, since the shore platforms formed since 6ka BP are uplifted onshore while the sea-level stabilization/slowdown periods alone during MIS1 were not sufficient for the formation of the terraces based on our model. However, it cannot be excluded that uplifting events might be responsible for sea-level slowdown, thus for the nearshore terrace sequence formation.

5.2.2. *"Distant" submarine terraces – towards a higher MIS3*

Our model showed that the most possible period for the distant STs formation was during the transition from MIS4 to MIS3 (~60ka BP) and during MIS3 highstands (Fig. 10). However, none of the existing RSLCs could justify the formation of all the distant STs after each test. The most successful of the RSLCs were able to form only 6 out of 7 STs. The reason why this happens is that despite using even short-term uplift rates (which are higher than the long-term) the MIS3 periods of sea-level slowdown or stabilization predicted from existing RSLCs are generally lower than the STs' depth.

Recently, Gowan et al., 2021 reconstructed the first pre-LGM global ice-sheet model and supported that the sea level during MIS3 was higher than what is already known by ocean $\delta^{18}O$ proxies. They support that it is highly doubtful that during MIS3 the sea level ranged from −60 to −90m. Instead, it is believed that it remained above −50m between 50 and 35ka BP with an abrupt shift to −25m. This is further supported by Pico et al. (2018), 2017, 2016 who calculated the sea level to have

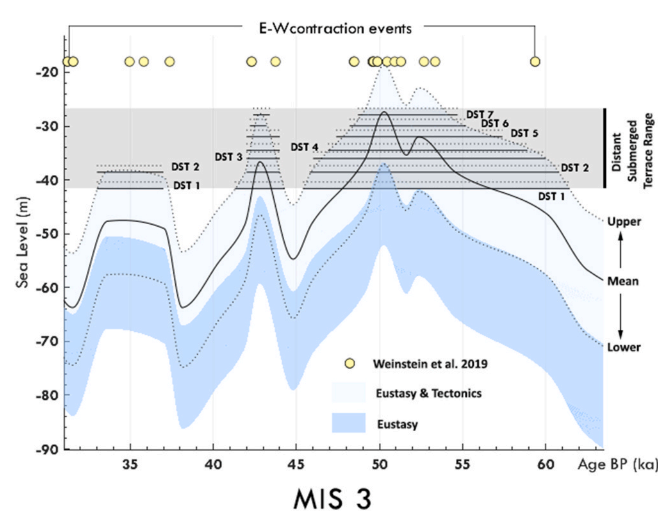

Fig. 11. Shifted sea-level curve of Siddall et al. (2003) (shifted for +5, +10, +15, +20, +25, +30 m) and comparison to the depth of the distant terrace sequence. The yellow points declare E-W contraction events and the activation of intense thrusting which is translated as uplifting events (Weinstein and Nuriel, 2019; Weinstein et al., 2020). (For interpretation of the references to color in this figure legend, the reader is referred to the Web version of this article.)

reached −40m during this period.

For this reason, we tested again our model for the already existing RSLCs but this time we shifted upwards each RSLC from +5 to +30m (Fig. 11-blue polygon), using a 5m interval, during the period between the glacial periods MIS2 and MIS4 (20-65ka BP, MIS3). Below are presented the shifted RSLCs (affected also by tectonics) for which the formation of the distant STs was the most successful (that of Siddall et al., 2003) (Fig. 11-light blue polygon), which also met the criteria for the formation of 7 out of 7 STs. During this part of the analysis, the best simulations explaining the formation of the distant STs within MIS 3 were achieved when the maximum eustatic sea level was at −37m, the CRR ranged between 0.09 m/a to 0.05 m/a and the uplift rate was between 0.28 and 0.38 mm/a. The RSLC of Grant et al., (2014) also reached a maximum eustatic sea level of −38m while it succeeded in reconstructing 6 out of 7 distant STs even for CRR range of 0.05–0.09 m/a. The successful uplift rates for this curve ranged from 0.28 to 0.34 mm/a.

The linear attribution of uplift rate to the RSLCs of course can be deceptive (Stocchi et al., 2018) since tectonic intensity (or activity) varies over time. However, the formation of the distant STs during the MIS 3 could be further supported by the regional tectonic activity which may have contributed to their preservation. U–Th datings from calcite-filled veins records in the Metulla block at the southern fringes of the Yammouneh fault (Weinstein and Nuriel, 2019; Weinstein et al., 2020), showed extensive growth of the veins from 53 to 16ka BP. This is tectonically translated to strong E-W contraction and activation of intense thrusting, which is responsible for the uplifting regime of our survey area. As seen in Fig. 11, the exact dates of these contraction events (yellow points) coincide with the periods when the formation of the distant STs was the most probable. Therefore, the formation of the distant STs during MIS3 is further supported by contraction events and relative vertical displacements of the ancient coastal zones, thereby allowing the terraces more time to be formed and also preserved. By taking this into account the distant STs were probably created into multiple sea-level stabilization phases and the most probable periods are those between the transition from MIS4 to MIS3 and MIS3 (~62-50ka BP), and also MIS3 sea-level highstands between 35 and 45ka BP.

5.3. Inheritance

Another factor that should be mentioned, is the possibility that the platforms were originally flattened during previous interglacial periods, which is called inheritance or reoccupation (Trenhaile, 1999). Our model was also tested for sea-level stabilization/slowdown up to MIS7. It was observed that the original creation of the STs might actually be polygenic since sea level might have originally shaped Lebanon's coast during the glacial period of MIS6. However, this hypothesis is highly debatable since the formation of terraces in uplifting areas is unfavored during glacial periods and because the rocky formations of the area should have been formed before MIS6, instead it appears that its genesis is very recent.

6. Conclusions

The current marine geophysical survey launches the beginning of offshore surveys on the Lebanese coast which are related to analysis and modeling of submerged relative sea-level indicators (RSLi), aiming to acquire information about paleo sea-level fluctuation. The coastal marine geophysical data presented herein are the first to date, that show the existence of well-shaped submarine terraces in Lebanon and the Eastern Mediterranean. Adding to its value, these RSLi were detected at the foot of one of the oldest known, continuously inhabited places in human history, the ancient city of Byblos (UNESCO World Heritage site, 1984). This work constitutes a first overall insight in the relative sea-level change indicators found at the central Lebanese coast. Finally, it proposes an integrated methodological approach for setting the most probable terrace formation time frame in the absence of dating material from the terraces.

The main results of the current survey are:

- Although the uplifting regime is not considered an advantage for the formation of paleo RSLi, the Lebanese coast is a promising area for studying them due to their precision (microtidal regime), and preservation (easily carved coastal limestone-sandstone, uplifting regime).
- Two different submarine terrace sequences were recognized: a) "distant" sequence within 40–25m below present sea level (distinct features), b) "nearshore" sequence 11.7–0.1m below present sea level (classic staircase sequence).
- In the absence of dating material, a model that uses existing relative sea-level curves and analyzes them for different uplift and cliff retreat rates was built to estimate the more possible terrace formation time frame. It was found that the nearshore sequence was originally formed during MIS5a sea-level highstand and possibly re-flattened during the first sea-level stabilization or slowdown periods of MIS1 (8-6ka BP). The distant sequence was formed within the MIS4 to MIS3 transition (~62-50ka BP), and during MIS3 sea-level highstands (35-45ka BP). These time frames were further supported by chronologically intercurrent uplifting events that facilitated the RSLi formation and preservation. To date, these submarine MIS3 RSLi are unique in the eastern Mediterranean.
- A long-term uplift rate of 0.28–0.37 mm/a best fit our data and also RSLi referred onshore. Long-term cliff retreat rates of 0.026 and 0.013 m/a were measured for Byblos and Anfeh respectively using GPS measurements, while our model was effective for cliff retreat rates from 0.03 to 0.09 m/a.
- Finally, our model supports recent ice-sheet reconstructions related to higher MIS3 values since sea-level curves that were tested for higher MIS3 values (eustatically reaching up to −37/−38m depth), proved more successful in the formation of the distant submarine terrace sequence.

Author contributions

Conceptualization: N.G., M.A., G.P., P.S; writing—original draft: N. G.; visualization: N.G.; funding acquisition: N.G.; survey planning: G.P., D.C., N.G.; fieldwork: N.G., M.G., M.A., D.C., X.D., Z.D., M.I., G.P.; project administration: M.A.; resources: G.P. and M.A.; marine geophysics data curation and processing: N.G., D.C.; software: N.G.; supervision: G.P., M.G.; validation: G.P., M.G, E.F.; writing—review and editing: G.P., P.S., M.G., M.A.;

Data availability

Data presented in this manuscript are available on request.

Funding

N.Georgiou was financially supported by the Hellenic Foundation for Research and Innovation (HFRI) and the General Secretariat for Research and Technology (GSRT), under the HFRI Ph.D. Fellowship grant (GA. no. 2560). Marine geophysical surveys are part of the multidisciplinary program "Byblos & the Sea" which began in 2011 and is under the direction of Nicolas Grimal and Martine Francis-Allouche.

Declaration of competing interest

The authors declare that they have no known competing financial interests or personal relationships that could have appeared to influence the work reported in this paper.

Acknowledgments

We would like to thank the divers Sahar Lakkis and Naim Solta for their help in the underwater surveys.

Appendix A. Supplementary data

Supplementary data to this article can be found online at https://doi.org/10.1016/j.quaint.2021.12.008.

References

Antonioli, F., Presti, V. Lo, Rovere, A., Ferranti, L., Anzidei, M., Furlani, S., Mastronuzzi, G., Orru, P.E., Scicchitano, G., Sannino, G., Spampinato, C.R., Pagliarulo, R., Deiana, G., Sabata, E. de, Sansò, P., Vacchi, M., Vecchio, A., 2015. Tidal notches in Mediterranean Sea: a comprehensive analysis. Quat. Sci. Rev. 119, 66–84. https://doi.org/10.1016/j.quascirev.2015.03.016.

Aoun, N.S., Harajli, H.A., Queffeulou, P., 2013. Preliminary appraisal of wave power prospects in Lebanon. Renew. Energy 53, 165–173. https://doi.org/10.1016/j.renene.2012.11.008.

Asmar, Chloe, Grasemann, Bernhard, Nader, Fadi, Tari, Gabor, 2013. The Qartaba Anticline (central Mount Lebanon): Implications for the tectonic evolution of onshore Lebanon. Geophysical Research Abstracts 15 (EGU20136740).

Avnaim-Katav, S., Almogi-Labin, A., Sandler, A., Sivan, D., Porat, N., Matmon, A., 2012. The chronostratigraphy of a quaternary sequence at the distal part of the nile littoral cell, Haifa Bay, Israel. J. Quat. Sci. 27, 675–686. https://doi.org/10.1002/jqs.2537.

Bailey, G., 2004. World prehistory from the margins: the role of coastlines in human evolution. J. Interdis. Stud. His. Archaeol. 1, 39–50.

Bailey, G.N., Flemming, N.C., 2008. Archaeology of the continental shelf : marine resources , submerged landscapes and underwater archaeology. Quat. Sci. Rev. 27, 2153–2165. https://doi.org/10.1016/j.quascirev.2008.08.012.

Barkai, O., Katz, O., Mushkin, A., Goodman-Tchernov, B.N., 2018. Long-term retreat rates of Israel's Mediterranean sea cliffs inferred from reconstruction of eroded archaeological sites. Geoarchaeology 33, 314–327. https://doi.org/10.1002/gea.21633.

Barlow, N.L.M., McClymont, E.L., Whitehouse, P.L., Stokes, C.R., Jamieson, S.S.R., Woodroffe, S.A., Bentley, M.J., Callard, S.L., Cofaigh, C.Ó., Evans, D.J.A., Horrocks, J.R., Lloyd, J.M., Long, A.J., Margold, M., Roberts, D.H., Sanchez-Montes, M.L., 2018. Lack of evidence for a substantial sea-level fluctuation within the Last Interglacial. Nat. Geosci. 11, 627–634. https://doi.org/10.1038/s41561-018-0195-4.

Benjamin, J., Rovere, A., Fontana, A., Furlani, S., Vacchi, M., Inglis, R.H., Galili, E., Antonioli, F., Sivan, D., Miko, S., Mourtzas, N., Felja, I., Meredith-Williams, M., Goodman-Tchernov, B., Kolaiti, E., Anzidei, M., Gehrels, R., 2017. Late Quaternary sea-level changes and early human societies in the central and eastern Mediterranean Basin: an interdisciplinary review. Quat. Int. https://doi.org/10.1016/j.quaint.2017.06.025.

Beydoun, Z.R., 1976. Observations on geomorphology, transportation and distribution of sediments in western Lebanon and its continental shelf and slope regions. Mar. Geol. 21, 311–324. https://doi.org/10.1016/0025-3227(76)90013-X.

Bilbao-Lasa, P., Jara-muñoz, J., Pedoja, K., Álvarez, I., 2020. Submerged Marine Terraces Identification and an Approach for Numerical Modeling the Sequence Formation in the Bay of Biscay (Northeastern Iberian Peninsula), 8, pp. 1–20. https://doi.org/10.3389/feart.2020.00047.

Boulton, S.J., Stewart, I.S., 2015. Holocene coastal notches in the Mediterranean region: indicators of palaeoseismic clustering? Geomorphology 237, 29–37. https://doi.org/10.1016/j.geomorph.2013.11.012.

Carton, H., Singh, S.C., Tapponier, P., Elias, A., Briais, A., Sursock, A., Jomaa, R., King, G.C.P., Daëron, M., Jacques, E., Barrier, L., 2009. Seismic evidence for Neogene and active shortening offshore of Lebanon (Shalimar cruise). J. Geophys. Res. 114 (B07407) https://doi.org/10.1029/2007JB005391.

Collina-Girard, J., 2002. Underwater mapping of Late Quaternary submerged shorelines in the western Mediterranean sea and Caribbean sea. Quat. Int. 92, 63–72. https://doi.org/10.1016/S1040-6182(01)00115-X.

Collina-Girard, J., Frost, Honor, 2002. Un promontoire sous- marin au large du port antique de Byblos: cartographie, interprétation géologique et implications archéologiques. Bulletin. Bulletin d'Archéol. et d'Architec. Liban. 6, 317–324. https://doi.org/10.1017/CBO9781107415324.004.

Daëron, Mathieu, Benedetti, Lucilla, Tapponnier, Paul, Sursock, Alexandre, Finkel, Robert C., 2004. Constraints on the post ~25-ka slip rate of the Yammoûneh fault (Lebanon) using in situ cosmogenic 36Cl dating of offset limestone-clast fans. Earth Planet Sci. Lett. 227 (1–2), 105–119. https://doi.org/10.1016/J.EPSL.2004.07.014.

de Lange, W.P., Moon, V.G., 2005. Estimating long-term cliff recession rates from shore platform widths. Eng. Geol. 80, 292–301. https://doi.org/10.1016/j.enggeo.2005.06.004.

Dodonov, A.E., Trifonov, V.G., Ivanova, T.P., Kuznetsov, V. Yu, Maksimov, F.E., Bachmanov, D.M., Sadchikova, T.A., Simakova, A.N., Minini, H., Al-Kafri, A.M., Ali, O., 2008. Late Quaternary marine terraces in the Mediterranean coastal area of Syria: Geochronology and neotectonics. Quat. Int. 190 (1), 158–170. https://doi.org/10.1016/J.QUAINT.2008.02.008.

Douka, K., Bergman, C.A., Hedges, R.E.M., Wesselingh, F.P., Higham, T.F.G., 2013. Chronology of Ksar Akil (Lebanon) and implications for the colonization of Europe by anatomically modern humans. PLoS One 8. https://doi.org/10.1371/journal.pone.0072931.

Dubertret, L., 1945. Jbail Detailed Surface Geology Map of Louis Dubertret. http://www.swaen.com/antique-map-of.php?id=1961.

Dubertret, L., 1954. Carte géologique au 1/200 feuille de Beyrouth avec notice explicative.

Dubertret, L., 1975. Introduction à la carte géologique à 1/50 000e. Notes et Mém. sur le Moyen-Orient, 13, pp. 345–402.

Dumas, Bernard, Guérémy, Pierre, Raffy, Jeannine, 2005. Evidence for sea-level oscillations by the "characteristic thickness" of marine deposits from raised terraces of Southern Calabria (Italy). Quat. Sci. Rev. 24 (18–19), 2120–2136. https://doi.org/10.1016/J.QUASCIREV.2004.12.011.

Dunand, M., 1949. Byblia grammata; documents et recherches sur le développement de l'écriture en Phénicie (Beirut).

Elias, A., Tapponnier, P., Singh, S.C., King, G.C.P., Briais, A., Daëron, M., Carton, H., Sursock, A., Jacques, E., Jomaa, R., Klinger, Y., 2007. Active thrusting offshore Mount Lebanon: source of the tsunamigenic A.D. 551 Beirut-Tripoli earthquake. Geology 35, 755–758. https://doi.org/10.1130/G23631A.1.

Faour, Ghaleb, Rizk, Elias Abi, 2008. Changes in the Lebanese Shoreline between 1962 and 2003. GEO OBSERVATEUR No 17.

Ferentinos, G., Fakiris, E., Christodoulou, D., Geraga, M., Dimas, X., Georgiou, N., Kordella, S., Papatheodorou, G., Prevenios, M., Sotiropoulos, M., 2020. Optimal sidescan sonar and subbottom profiler surveying of ancient wrecks: the 'Fiskardo' wreck, Kefallinia Island, Ionian Sea. J. Archaeol. Sci. 113, 105032. https://doi.org/10.1016/j.jas.2019.105032.

Fleisch, H., Sanlaville, P., 1974. La Plage de + 52 m et son Acheuléen à Ras Beyrouth et à l'Ouadi Aabet (Liban). Paleorient 2, 45–85. https://doi.org/10.3406/paleo.1974.4174.

Francis-Allouche, Martine, et al., 2017. Byblos maritime : une installation portuaire au piémont sud de la ville antique BAAL, pp. 197–262.

Frost, H., 1998. Marine prospection at Byblos. BAAL 3, 245–259.

Frost, H., 2002. Four season of marine investigation: preliminary charting of the offshore shallows. BAAL 6, 309–316.

Frost, H., 2004. Byblos and the Sea, A Decade O. Ed. Lebanese British Friends of the National Museum.

Furlani, S., Pappalardo, M., Gómez-Pujol, L., Chelli, A., 2014. The rock coast of the Mediterranean and Black seas. Geol. Soc. Memoir. 40, 89–123. https://doi.org/10.1144/M40.7.

Galili, E., Zviely, D., Ronen, A., Mienis, H.K., 2007. Beach deposits of MIS 5e high sea stand as indicators for tectonic stability of the Carmel coastal plain, Israel. Quat. Sci. Rev. 26, 2544–2557. https://doi.org/10.1016/j.quascirev.2007.06.027.

Galili, E., Nir, Y., Vachtman, D., Mart, Y., 2017. Physical Characteristics of the Continental Shelves of the East Mediterranean Basin. Submerged Landscapes of the European Continental Shelf. Wiley Online Books. https://doi.org/10.1002/9781118927823.ch14.

Georgiou, N., Papatheodorou, G., Geraga, M., Christodoulou, D., 2018. Marine Geo-Archaeological Survey in Byblos. Lebanon , Eastern Mediterranean.

Georgiou, N., Stocchi, P., Rovere, A., Casella, E., 2020. Reconstructing Past Sea Level through Notches. Orosei Gulf.

Georgiou, N., Dimas, X., Fakiris, E., Christodoulou, D., Geraga, M., Koutsoumpa, D., Baika, K., Kalamara, P., Ferentinos, G., Papatheodorou, G., 2021a. A Multidisciplinary Approach for the Mapping, Automatic Detection and Morphometric Analysis of Ancient Submerged Coastal Installations: the Case Study of the Ancient Aegina Harbour Complex. Remote Sensing MDPI submitted in.

Georgiou, N., Dimas, X., Papatheodorou, G., 2021b. Integrated Methodological Approach for the Documentation of Marine Priority Habitats and Submerged Antiquities: Examples from the Saronic Gulf, Greece. Sustainability In Press.

Geraga, M., Papatheodorou, G., Ferentinos, G., Fakiris, E., Christodoulou, D., Georgiou, N., Dimas, X., Iatrou, M., Kordella, S., Sotiropoulos, G., Mentogiannis, V., Delaporta, K., 2015. The study of an ancient shipwreck using marine remote sensing techniques. Archaeol. Marit. Med. 12. Kefalonia Island (Ionian Sea), Greece.

Geraga, M., Christodoulou, D., Eleftherakis, D., Papatheodorou, G., Fakiris, E., Dimas, X., Georgiou, N., Kordella, S., Prevenios, M., Iatrou, M., Zoura, D., Kekebanou, S., Sotiropoulos, M., Ferentinos, G., 2020. Atlas of shipwrecks in inner ionian sea (Greece): a remote sensing approach. Heritage 3, 1210–1236. https://doi.org/10.3390/heritage3040067.

Gomez, F., Nemer, T., Tabet, C., Khawlie, M., Meghraoui, M., Barazangi, M., 2007. Strain Partitioning of Active Transpression within the Lebanese Restraining Bend of the Dead Sea Fault (Lebanon and SW Syria), 290. Geological Society, London, Special Publications, pp. 285–303. https://doi.org/10.1144/290.10.

Gowan, E.J., Zhang, X., Khosravi, S., Rovere, A., Stocchi, P., Hughes, A.L.C., Gyllencreutz, R., Mangerud, J., Svendsen, J., Lohmann, G., 2021. A new global ice sheet reconstruction for the past 80 000 years. Nat. Commun. 1–9. https://doi.org/10.1038/s41467-021-21469-w.

Gracia, F.J., Rodríguez-Vidal, J., Cáceres, L.M., Belluomini, G., Benavente, J., Alonso, C., 2008. Diapiric uplift of an MIS 3 marine deposit in SW Spain: Implications for Late Pleistocene sea level reconstruction and palaeogeography of the Strait of Gibraltar. Quat. Sci. Rev. 27 (23–24), 2219–2231. https://doi.org/10.1016/J.QUASCIREV.2008.08.013.

Grant, K.M., Rohling, E.J., Bronk Ramsey, C., Cheng, H., Edwards, R.L., Florindo, F., Heslop, D., Marra, F., Roberts, A.P., Tamisiea, M.E., Williams, F., 2014. Sea-level variability over five glacial cycles. Nat. Commun. 5 https://doi.org/10.1038/ncomms6076.

Grimal, N., 2009. « Quelques réflexions sur la géopolitique du Levant au deuxième millénaire av. J.C.», in Interconnections in the Eastern Mediterranean Lebanon in the Bronze and Iron Ages. BAAL HS 339–360.

Gzam, M., Mejdoub, N. El, Jedoui, Y., 2016. Late quaternary sea level changes of gabes coastal plain and shelf: identification of the MIS 5c and MIS 5a onshore highstands, Southern Mediterranean. J. Earth Sys. Sci. 125, 13–28. https://doi.org/10.1007/s12040-015-0649-7.

Hall, J.W., Meadowcroft, I.C., Lee, E.M., Gelder, P.H.A.J.M. Van, 2002. Stochastic simulation of episodic soft coastal cliff recession. Coast Eng. 46, 159–174. https://doi.org/10.1016/S0378-3839(02)00089-3.

Hwan, C., Park, J.W., Lee, M.H., Park, C.H., Kim, C.H., Park, J.W., Lee, M.H., Park, C.H., 2013. Detailed bathymetry and submarine terraces in the coastal area of the dokdo volcano in the ulleung basin , the east sea (sea of Japan) detailed bathymetry and submarine terraces in the coastal area of the dokdo volcano in the ulleung basin. Near East 65, 523–528. https://doi.org/10.2112/SI65-089.1.

Jara-Muñoz, J., Melnick, D., Pedoja, K., Strecker, M.R., 2019. TerraceM-2: a Matlab® interface for mapping and modeling marine and lacustrine terraces. Front. Earth Sci. 7, 1–18. https://doi.org/10.3389/feart.2019.00255.

Jidejian, N., 1971. Byblos through the Ages. Librairie Orientale, Beirut.

Kabbara, N., Sorgente, R., Natale, S., Hayes, D.R., Zodiatis, G., 2006. High-resolution Nested Model for the Lebanese Coastal Area , Eastern Mediterranean : Implementation and Climatological Runs, pp. 373–396.

Kennedy, D.M., 2016. The subtidal morphology of microtidal shore platforms and its implication for wave dynamics on rocky coasts. Geomorphology 268, 146–158. https://doi.org/10.1016/j.geomorph.2016.06.003.

Kennedy, D.M., Stephenson, W.J., Naylor, L.A., 2014. Introduction to the rock coasts of the world. Geol. Soc. Memoir. 40, 1–5. https://doi.org/10.1144/M40.1.

Lafont, B., 2009. D'Ur à Byblos : les relations entre la Mésopotamie et le Levant aux Âges du Bronze Ancien et Moyen. L'apport des textes. In: Proceedings of the International Symposium Beirut, BAAL HS VI, pp. 91–106.

Leroi-Gourhan, A., 1980. Les analyses polliniques au Moyen-Orient. Paleorient 6, 79–91. https://doi.org/10.3406/paleo.1980.4261.

Lorscheid, T., Rovere, A., 2019. The Indicative Meaning Calculator – Quantification of Paleo Sea-Level Relationships by Using Global Wave and Tide Datasets 8.

Matsumoto, H., Dickson, M.E., Masselink, G., 2017a. Geomorphology Systematic analysis of rocky shore platform morphology at large spatial scale using LiDAR-derived digital elevation models. Geomorphology 286, 45–57. https://doi.org/10.1016/j.geomorph.2017.03.011.

Matsumoto, H., Dickson, M.E., Masselink, G., 2017b. Systematic analysis of rocky shore platform morphology at large spatial scale using LiDAR-derived digital elevation models. Geomorphology 286, 45–57. https://doi.org/10.1016/j.geomorph.2017.03.011.

Micallef, A., Foglini, F., Le, T., Angeletti, L., Maselli, V., Pasuto, A., Taviani, M., 2013. The submerged paleolandscape of the Maltese Islands : morphology , evolution and relation to Quaternary environmental change. Mar. Geol. 335, 129–147. https://doi.org/10.1016/j.margeo.2012.10.017.

Morhange, C., Pirazzoli, P.A., Marriner, N., Montaggioni, L.F., Nammour, T., 2006. Late Holocene Relative Sea-level changes in Lebanon, eastern mediterranean. Mar. Geol. 230, 99–114. https://doi.org/10.1016/j.margeo.2006.04.003.

Mushkin, A., Katz, O., Porat, N., 2019. Overestimation of short-term coastal cliff retreat rates in the eastern Mediterranean resolved with a sediment budget approach. Earth Surf. Process. Landforms 44, 179–190. https://doi.org/10.1002/esp.4490.

Nader, F.H., 2011. The petroleum prospectivity of Lebanon: an overview. J. Petrol. Geol. 34, 135–156. https://doi.org/10.1111/j.1747-5457.2011.00498.x.

Papatheodorou, G., Geraga, M., Georgiou, N., Christodoulou, D., Mathé, V., 2017. Byblos maritime : une installation portuaire au piémont sud de la ville antique.

Nader, F.H., Browning-Stamp, P., Lecomte, J.C., 2016. Geological interpretation of 2D seismic reflection profiles onshore lebanon: implications for petroleum exploration. J. Petrol. Geol. 39 (4), 333–356. https://doi.org/10.1111/jpg.12656.

Papatheodorou, G., Geraga, M., Christodoulou, D., Fakiris, E., Iatrou, M., Georgiou, N., Dimas, X., Ferentinos, G., 2021. The battle of lepanto search and survey mission (1971–1972) by throckmorton, edgerton and yalouris: following their traces half a century later using marine geophysics. Rem. Sens. https://doi.org/10.3390/rs13163292.

Passaro, S., Ferranti, L., Alteriis, G. De, 2011. The use of high-resolution elevation histograms for mapping submerged terraces : tests from the Eastern Tyrrhenian Sea and the Eastern Atlantic Ocean. Quat. Int. 232, 238–249. https://doi.org/10.1016/j.quaint.2010.04.030.

Pedoja, K., Husson, L., Johnson, M.E., Melnick, D., Witt, C., Pochat, S., Nexer, M., Delcaillau, B., Pinegina, T., Poprawski, Y., Authemayou, C., Elliot, M., Regard, V., Garestier, F., 2014. Coastal staircase sequences reflecting sea-level oscillations and tectonic uplift during the Quaternary and Neogene. Earth Sci. Rev. 132, 13–38. https://doi.org/10.1016/j.earscirev.2014.01.007.

Pico, T., Mitrovica, J.X., Ferrier, K.L., Braun, J., 2016. Global ice volume during MIS 3 inferred from a sea-level analysis of sedimentary core records in the Yellow River Delta. Quat. Sci. Rev. 152, 72–79. https://doi.org/10.1016/j.quascirev.2016.09.012.

Pico, T., Creveling, J.R., Mitrovica, J.X., 2017. sea-Level records from the U.S. Mid-atlantic constrain laurentide ice sheet extent during marine isotope stage 3. Nat. Commun. 8, 1–6. https://doi.org/10.1038/ncomms15612.

Pico, T., Birch, L., Weisenberg, J., Mitrovica, J.X., 2018. Refining the Laurentide Ice Sheet at Marine Isotope Stage 3: a data-based approach combining glacial isostatic simulations with a dynamic ice model. Quat. Sci. Rev. 195, 171–179. https://doi.org/10.1016/j.quascirev.2018.07.023.

Pirazzoli, P.A., 2005. A review of possible eustatic, isostatic and tectonic contributions in eight late-Holocene relative sea-level histories from the Mediterranean area. Quat. Sci. Rev. 24 (18–19), 1989–2001. https://doi.org/10.1016/J.QUASCIREV.2004.06.026.

Pirazzoli, P.A., Laborel, J., Saliège, J.F., Erol, O., Kayan, I., Person, A., 1991. Holocene raised shorelines on the Hatay coasts (Turkey): palaeoecological and tectonic implications. Mar. Geol. 96, 295–311. https://doi.org/10.1016/0025-3227(91)90153-U.

Plassard, J., Kogoj, B., 1981. Séismicité du Liban, 47. Conseil National de la Recherche Scientifique, Beirut.

Porat, N., Avital, A., Frechen, M., Almogi-Labin, A., 2003. Chronology of upper Quaternary offshore successions from the southeastern Mediterranean Sea, Israel. Quat. Sci. Rev. 22, 1191–1199. https://doi.org/10.1016/S0277-3791(03)00016-7.

Potter, E.K., Esat, T.M., Schellmann, G., Radtke, U., Lambeck, K., McCulloch, M.T., 2004. Suborbital-period sea-level oscillations during marine isotope substages 5a and 5c. Earth Planet Sci. Lett. 225, 191–204. https://doi.org/10.1016/j.epsl.2004.05.034.

Prémaillon, M., Regard, V., Dewez, T.J.B., Auda, Y., 2018. GlobR2C2 (Global Recession Rates of Coastal Cliffs): a global relational database to investigate coastal rocky cliff erosion rate variations. Earth Surf. Dyn. 6, 651–668. https://doi.org/10.5194/esurf-6-651-2018.

Reilinger, R., McClusky, S., Vernant, P., Lawrence, S., Ergintav, S., Cakmak, R., Ozener, H., et al., 2006. GPS constraints on continental deformation in the Africa-Arabia-Eurasia continental collision zone and implications for the dynamics of plate interactions. J. Geophys. Res. Solid Earth 111 (5). https://doi.org/10.1029/2005JB004051.

Rohling, E.J., Foster, G.L., Grant, K.M., Marino, G., Roberts, A.P., Tamisiea, M.E., Williams, F., 2014. Sea-level and deep-sea-temperature variability over the past 5.3 million years. Nature. https://doi.org/10.1038/nature13230.

Rovere, A., Vacchi, M., Firpo, M., Carobene, L., 2011. Underwater geomorphology of the rocky coastal tracts between finale ligure and vado ligure (western liguria, NW Mediterranean sea). Quat. Int. 232, 187–200. https://doi.org/10.1016/j.quaint.2010.05.016.

Rovere, A., Raymo, M.E., Vacchi, M., Lorscheid, T., Stocchi, P., Gómez-pujol, L., Harris, D.L., Casella, E., Leary, M.J.O., Hearty, P.J., 2016a. Earth-Science Reviews the analysis of Last Interglacial (MIS 5e) relative sea-level indicators : reconstructing sea-level in a warmer world. Earth Sci. Rev. 159, 404–427. https://doi.org/10.1016/j.earscirev.2016.06.006.

Rovere, A., Stocchi, P., Vacchi, M., 2016b. Eustatic and relative sea level changes. Curr. Clim. Change Rep. 2, 221–231. https://doi.org/10.1007/s40641-016-0045-7.

Rovere, A., Raymo, M.E., Vacchi, M., Lorscheid, T., Stocchi, P., Gómez-Pujol, L., Harris, D.L., Casella, E., O'Leary, M.J., Hearty, P.J., 2016c. The analysis of Last Interglacial (MIS 5e) relative sea-level indicators: reconstructing sea-level in a warmer world. Earth Sci. Rev. https://doi.org/10.1016/j.earscirev.2016.06.006.

Sanlaville, P., 1969. Les bas niveaux marins pléistocènes du Liban. Méditerranée 10, 257–292. https://doi.org/10.3406/medit.1969.1322.

Schellmann, G., Radtke, U., Potter, E.K., Esat, T.M., McCulloch, M.T., 2004. Comparison of ESR and TIMS U/Th dating of marine isotope stage (MIS) 5e, 5c, and 5a coral from Barbados-implications for palaeo sea-level changes in the Caribbean. Quat. Int. 120, 41–50. https://doi.org/10.1016/j.quaint.2004.01.005.

Siddall, M., Rohling, E.J., Almogi-Labin, A., Hemleben, C., Meischner, D., Schmelzer, I., Smeed, D.A., 2003. Sea-level fluctuations during the last glacial cycle. Nature 423, 853–858. https://doi.org/10.1038/nature01690.

Siddall, M., Rohling, E.J., Thompson, W.G., Waelbroeck, C., 2008. Marine isotope stage 3 sea level fluctuations: data synthesis and new outlook. Rev. Geophys. 46, 1–29. https://doi.org/10.1029/2007RG000226.

Sivan, D., Wdowinski, S., Lambeck, K., Galili, E., Raban, A., 2001. Holocene sea-level changes along the Mediterranean coast of Israel, based on archaeological observations and numerical model. Palaeogeogr. Palaeoclimatol. Palaeoecol. 167, 101–117. https://doi.org/10.1016/S0031-0182(00)00234-0.

Sivan, D., Schattner, U., Morhange, C., Boaretto, E., 2010. What can a sessile mollusk tell about neotectonics. Earth Planet Sci. Lett. 296, 451–458. https://doi.org/10.1016/j.epsl.2010.05.032.

Stephenson, W.J., 2000. Shore platforms: a neglected coastal feature? Prog. Phys. Geogr.: Earth Environ. 24, 311–327. https://doi.org/10.1177/030913330002400301.

Stephenson, W., 2001. Shore platform width - a fundamental problem. Z. fur. Geomorphol. 45, 511–527.

Stocchi, P., Vacchi, M., Lorscheid, T., Boer, de Boer, Simms, A.R., Van de Wal, R.S.W., Vermeersen, B.L.A., Pappalardo, M., Rovere, A., 2018. MIS 5e relative sea-level changes in the Mediterranean Sea: contribution of isostatic disequilibrium. Quat. Sci. Rev. 185, 122–134. https://doi.org/10.1016/j.quascirev.2018.01.004.

Sunamura, T., 2015. Rocky coast processes: with special reference to the recession of soft rock cliffs. Proc. Jpn. Acad. Ser. B Phys. Biol. Sci. 91, 481–500. https://doi.org/10.2183/pjab.91.481.

Surić, M., Richards, D.A., Hoffmann, D.L., Tibljaš, D., Juračić, M., 2009. Sea-level change during MIS 5a based on submerged speleothems from the eastern Adriatic Sea (Croatia). Mar. Geol. 262, 62–67. https://doi.org/10.1016/j.margeo.2009.03.005.

Tarı, Ufuk, Tüysüz, Okan, Blackwell, Bonnie A.B., Mahmud, Zarrin, Florentin, Jonathan A., Qi, Justin, Genç, Can, Skinner, Anne R., 2018. Sea level change and tectonic uplift from dated marine terraces along the eastern Mediterranean coast, southeastern Turkey. Palaeogeogr., Palaeoclimatol., Palaeoecol. 511, 80–102. https://doi.org/10.1016/J.PALAEO.2018.07.003.

Trenhaile, A.S., 1999. The width of shore platforms in Britain, Canada, and Japan. J. Coast Res. 15, 355–364.

Trenhaile, A.S., 2000. Modeling the development of wave-cut shore platforms. Mar. Geol. 166, 163–178. https://doi.org/10.1016/S0025-3227(00)00013-X.

Trenhaile, A.S., 2001. Modeling the effect of weathering on the evolution and morphology of shore platforms. J. Coast Res. 17, 398–406.

Trenhaile, A.S., 2002a. Modeling the development of marine terraces on tectonically mobile rock coasts. Mar. Geol. https://doi.org/10.1016/S0025-3227(02)00187-1.
Trenhaile, A.S., 2002b. Rock coasts, with particular emphasis on shore platforms. Geomorphology 48, 7–22. https://doi.org/10.1016/S0169-555X(02)00173-3.
Trenhaile, A., 2006. Tidal wetting and drying on shore platforms: an experimental study of surface expansion and contraction. Geomorphology 76, 316–331. https://doi.org/10.1016/j.geomorph.2005.11.006.
Trenhaile, A.S., 2015. Earth-Science Reviews Coastal notches : their morphology , formation , and function. Earth Sci. Rev. 150, 285–304. https://doi.org/10.1016/j.earscirev.2015.08.003.
Waelbroeck, C., Labeyrie, L., Michel, E., Duplessy, J.C., McManus, J.F., Lambeck, K., Balbon, E., Labracherie, M., 2002. Sea-level and deep water temperature changes derived from benthic foraminifera isotopic records. Quat. Sci. Rev. 21, 295–305. https://doi.org/10.1016/S0277-3791(01)00101-9.
Weinstein, Y., Nuriel, P., 2019. Stable Isotopes of Calcite-Filled Veins and Ar-Ar of Associated Basalts from the Dead Sea Transform Fault, Version 1.0. Interdisciplinary Earth Data Alliance.
Weinstein, Y., Nuriel, P., Inbar, M., Jicha, B.R., Weinberger, R., 2020. Impact of the dead sea transform kinematics on adjacent volcanic activity. Tectonics 39, 1–17. https://doi.org/10.1029/2019TC005645.
Young, A.P., Carilli, J.E., 2019. Global distribution of coastal cliffs. Earth Surf. Process. Landforms 44, 1309–1316. https://doi.org/10.1002/esp.4574.
Zaatari, S. El, 2018. The central Levantine corridor: the Paleolithic of Lebanon. Quat. Int. 466, 33–47. https://doi.org/10.1016/j.quaint.2017.06.047.